論文 / 著書情報
Article / Book Information

題目(和文)	健診に利用可能な小口径全身PET装置の開発可能性に関する研究
Title(English)	Research on Feasibility of Small Diameter Entire-Body PET for a Physical Examination
著者(和文)	イスメットイスナイに
Author(English)	Ismet Isnaini
出典(和文)	学位:博士(工学), 学位授与機関:東京工業大学, 報告番号:甲第9597号, 授与年月日:2014年6月30日, 学位の種別:課程博士, 審査員:小尾　高史,大山　永昭,長橋　宏,熊澤　逸夫,山口　雅浩,山谷　泰賀
Citation(English)	Degree:Doctor (Engineering), Conferring organization: Tokyo Institute of Technology, Report number:甲第9597号, Conferred date:2014/6/30, Degree Type:Course doctor, Examiner:,,,,,
学位種別(和文)	博士論文
Type(English)	Doctoral Thesis

Research on Feasibility of Small Diameter Entire-Body PET for a Physical Examination

Thesis Advisor
Takashi Obi

A dissertation presented
By
Ismet Isnaini

To
The Department of Information Processing
In partial fulfillment of the requirements
For the degree of
Doctor of Engineering

In the subject of
Engineering

Interdisciplinary Graduate School of Science and Engineering
Tokyo Institute of Technology

ACKNOWLEDGEMENT

This research has been conducted in collaboration with National Institute of Radiological Sciences (NIRS) in Chiba , under the supervision of Dr. Eiji Yoshida and Dr. Taiga Yamaya

Table of Content

Chapter 5 Evaluation of Entire-body PET with Several Ring Diameters

List of Figures

List of Tables

Chapter 1

Introduction

1.1. Positron Emission Tomography (PET)

Positron Emission Tomography (PET) is a nuclear imaging technique which produce images that show anatomical structure as well as how certain tissues are performing their physiological functions. However, unlike X-ray or MR imaging, the main emphasis in PET is on functional imaging as its major modality. Specifically, PET studies evaluate the metabolism of a particular organ or tissue, so that information about the physiology (functionality) and anatomy (structure) of the organ or tissue is evaluated, as well as its biochemical properties. Thus,

PET may detect biochemical changes in an organ or tissue that can identify the onset of a disease process before anatomical changes related to the disease can be seen with other imaging processes, such as computed tomography (CT) or magnetic resonance imaging (MRI).

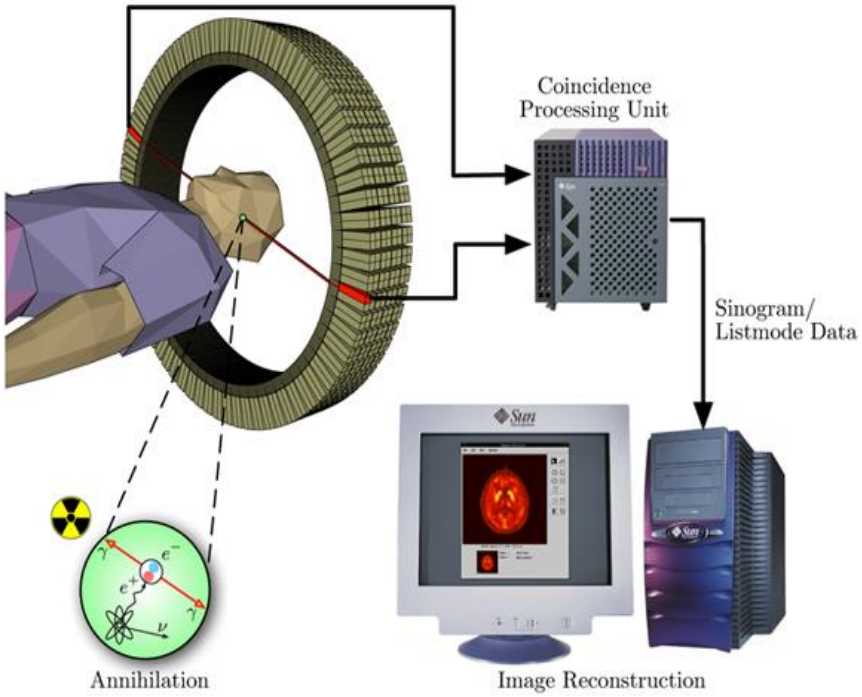

Figure 1 Positron Emission Tomography scanner system up to Image Reconstruction

Radionuclides are injected to the body as labels on tracer molecules designed to probe physiological processes. The radionuclide will be allowed to concentrate in the organ or tissue for about 30 to 60 minutes. It will not be hazardous to other people, as the radionuclide emits less radiation than a standard X-ray. These radioactive nuclei emit positrons that annihilate with electrons in the tissue. An annihilation event may result in two gamma photons being emitted in almost exactly 180 degrees and with an energy of 511 keV each. The gamma photons are

detected in coincidence in a detector ring (or several detector rings) so that two detected gamma photons represent a straight line along which the coincidence event took place, which is called Line Of Response (LOR). These lines are then gathered and processed with the aid of image processing tools to finally produce an image of the activity and thereby of the functionality.

1.2. Coincidence Events

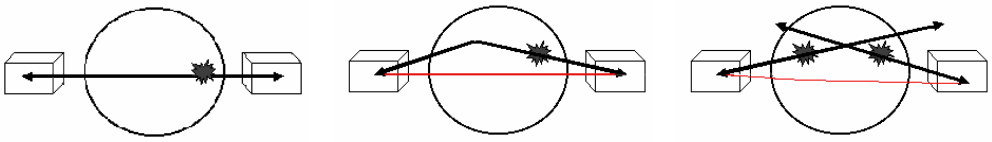

Figure 2 Types of coincidences events: True event (left), scatter event (center) and random event (right)

There are 3 kinds of coincidence events which form an LOR in a PET scanner. The left figure above, described a true coincidence events. This event occurs when both photons from an annihilation event are detected by detectors in coincidence time window and neither photon undergoes any form of interaction prior to detection, and no other event is detected within the coincidence time-window.

Figure 2 (center) described scatter events, which are formed when one of the photon undergoes at least one Compton scattering, prior to detection. The direction of the photon will be changed, and likely it will form a wrong LOR. These events will reduce spatial resolution, decreasing contrast and causing the isotope concentrations to be overestimated.

Random events are generated from 2 different sources, whose photons happened to be in the same LOR within coincidence time window of the system, as described in Figure 2 (right). These last two coincidence events are undesirable, since it will introduce noise and hence hamper the image reconstruction process. These events are dependents on many factor, one of them is the geometry of the scanner.

1.3. Aim of Research

The aim of this research is to design and simulate a PET scanner with an extended axial field of view (FOV), which can maintain a high performance in terms of true count rate (sensitivity) and count rate ratio between true, scattering and random coincidence events.

1.4. Structure of the Thesis

This thesis will be divided into several chapters:

- Background of research on Entire-body PET and its application on Cancer screening test is discussed in Chapter 2. Study on sensitivity and noise count rate ratio (NECR) is also explained.
- Evaluation Method and preliminary setup for simulation (Chapter 3)
- Simulation on entire-body PET with conventional and modified length as well as diameter (Chapter 4)

- Simulation on entire-body PET with different diameter length, and various study of single-data loss due to dead-time (Chapter 5)
- Discussions on pros and cons on entire-body PET for physical examination (Chapter 6)
- Conclusion (Chapter 7)

In chapter 2 we discuss the background of this research, as well as the need of entire-body PET. The application of PET scanner in Japan Cancer screening test is also described, and the current problems arises from such test is explained. In this chapter we also define our research goals and various methods to achieve them.

In Chapter 3 we describe the evaluation standard of the PET scanner performance in which this research will be based on. We also define the sensitivity and Noise Equivalent Noise Ratio (NECR) tests as our focus of study and describe what other factors might influences these values. The geometry structure of a PET scanner is described and explanation on (Depth Of Interaction) DOI-PET detector is given, with a little bit introduction of jPET-d4 scanner as the basic geometry of this research. In the same chapter, we give detail on the software and other supporting program used in the simulation, as well as the steps taken place during the simulation. This chapter also describes some preliminary simulations need to be taken, which were performed before the main simulation, in order to set the required parameters.

The following chapter describes the procedure taken in the sensitivity and NECR

test, as well as the different geometry and parameters applied in simulation of the conventional and axially extended FOV PET scanner. Two major simulations were conducted, namely one with standard diameter size and another with smaller diameter. A brief discussion on the result for different geometry in terms of sensitivity and NECR values, were discussed at the end of the chapter.

Chapter 5 describes the study and results on sensitivity and count rate performance tests using 4 different scanner diameters (biggest to smallest) with 4 axial FOV-length. We also discuss the single-data loss which cause by dead-time which affect the performance of entire-body PET scanner. Some solutions to reduce this affect were also offered. Several methods to reduce the total crystal volume employed in a scanner in order to minimize the production costs are also elaborated.

More detail arguments on pros and cons in entire-body PET scanner and its application on physical examination is discussed in chapter 6 of the book. Many different problems arise due to the extension of axial FOV are mentioned and solutions of such problems are suggested. Finally, the chapter 7 of this book points out the conclusion of this research.

Chapter 2

Background

2.1. Entire-body PET

Currently, clinical positron emission tomography (PET) scanners have about 20-cm axial field-of-view (FOV). These PET scanners image the whole body using six or more bed positions. On the other hand, an entire-body PET scanner with an extended axial FOV, which can trace whole-body uptake images at the same time and improve sensitivity dynamically, has been desired [1-2]. In other words, the entire whole-body PET scanner can reduce scan time dramatically. Eriksson et al. [3-4] have reported feasibility of PET scan time of sub-minutes using the extended axial FOV and time-of-flight (TOF) information. This PET

scanner may be cost effective for clinical PET scanners with high scan throughput.

However, PET detectors are main cause for the high cost of PET scanner even up to now. Some researchers have reported the entire-body PET scanners with cheap detectors and thin scintillation detectors to reduce PET scanner cost [5,6], unfortunately the efficiency of such detector is pretty low for low energy. Also, the entire-body PET scanner would have to process a large amount of data compared to conventional PET scanners, hence would hamper the image construction process.

The entire-body PET scanner also has many oblique line-of-responses (LORs). Several characteristics of oblique LORs, such as poor spatial resolution and decreased sensitivity due to smaller solid angle fraction and increased scatter fraction and attenuation [7], should be carefully discussed. Nevertheless, Oblique LORs are able to maintain high spatial resolution using a depth-of-interaction (DOI) detector [8-10].

2.2. Entire-body vs Whole-body PET

The term “whole-body PET” has been widely recognized. However, we would like to differentiate our system of “entire-body PET”, with the common term “whole-body PET”. A “whole-body PET” term is referring to PET scanner with any axial length which is used in a whole-body imaging process. Therefore it

might take several bed steps to perform such scan. Whereas our system of "entire-body PET" is a scanner which covers the whole-body of a patient (we assume the average human body size as 175 cm height) which can scan the whole-body in one bed position. Hence, in the rest of this paper, the Entire-body PET is referring to a system whose axial FOV length is about 200 cm.

Figure 3 Various whole-body PET (or PET/CT) scanner with short axial FOV, employed in a whole-body scanning. It does not cover the whole-body, therefore need several bed-step to perform whole-body scan.

2.3. PET Cancer Screening

In Japan, one of the major applications of PET scanner is the cancer screening test. Between 2006 and 2009, the government has conducted the "FDG-PET cancer screening program" [11-14], in which almost 40% of the patient has been examined using a dedicated PET scanner, while the rest were using a PET/CT. The dedicated scanner is known to have lower effective dose of 4.4 mSv (male 4.7 mSv; female 4.0 mSv) or equal to a constant injected dose of 216.8 MBq or variable injected dose of 3.7 MBq/kg or 261 MBq (for men) or 205 MBq (for women). The counter part of PET/CT is using an effective dose of 13.5 mSv (male 14.2 mSv; female 12.8 mSv) or equal to a variable injected dose of 3.6 MBq/kg or

252 MBq (for men) or 198 (for women). Recent study of cancer using a dedicated CT scan is taking about 5 min scanning time with effective dose of 10mSV.

Even though these values are still under the permissible safe limit per year for a radiation worker (50mSV) [15], however there has been some issue in regard to this screening test. First of all, some cancer cannot be detected during first screening test. Therefore, the need of repeated test at an appropriate time has arisen which also mean a repeated radiation exposure for a patient. Another problem is the radiation exposure itself. According to the International Commission on Radiation Protection (ICRP), the estimated cancer incidence induced by radiation exposure was 0.0048 % per mSv [16]. Cost, is another major problem. To minimize the cost, a combined screening test should be performed together along the screening cancer test.

One of the solutions of these problems is to reduce the amount of dose injected to the patient. This can only be possible, only when the scanner can produce high sensitivity image even at a low dose. With the entire-body PET which promising a high sensitivity, these dose can be suppressed to a level which is safe for patient even though need to repeated several time and at the same time producing a high sensitivity data which leads to an accurate cancer analysis.

2.4. Research Goal

The aim of the research is to design and evaluate such a scanner which can satisfy the following requirements:

- The length of the axial FOV should cover the whole body to be able to perform one-bed scanning dynamically. With an average human body height of 175 cm, we need to extend the axial FOV up to 2 m
- Current whole-body scan is mostly using conventional PET, which would require almost 30 minutes time acquisition, excluding the time between injecting radionuclide to the actual scanning itself. Our scanner should minimize scanning time less than 5 min per patient.
- The major problem of entire body PET scanner is the production cost. Our design should develop such scanner with less production cost. This could be achieved by reducing crystal volume used in the scanner geometry.
- The design of the scanner should ensure that with low injected dose, it can give an optimal performance. In other words, the radiation exposure caused by repeated use of such scanner, would not exceed the safety limit radiation exposure for a patient.
- The scanner should be directly or indirectly supports a cost-effective, less-harm cancer screening test.

Chapter 3

Evaluation Methods

3.1. Background

There are many factors which indicate the performance of a PET scanner. Some of these are spatial resolution, sensitivity and count rate performance. Spatial resolution is the ability of a scanner to clearly depicting two different points distinctively in a radiation distribution. In can also defined as the minimum distance between two points such that it can be detected by scanner.

Other important features are sensitivity and count rate performance. These two characteristics will be mostly discussed in this paper, in relation to the performance of the entire-body PET.

3.2. Performance Measurement Standard

National Electrical Manufacturers Associations (NEMA) has defined several standards in evaluating the performance of medical equipment such as PET scanner. The NEMA NU-2-2007 is the latest standard of NEMA on performance test on a brain dedicated PET scanner [17]. None of these standards have been validated against an entire-body PET. However, several of its methods will be used here to observe the performance of the proposed entire-body PET, with some modifications to suit the geometry of entire-body PET.

Several points are to be evaluated based on this standard:

- Spatial Resolution
- Scatter Fraction, Count Losses and Random Measurements
- Sensitivity
- Accuracy : Correction for Count losses and Random
- Image Quality, Accuracy for Attenuation and Scatter Corrections

However, our research is focusing on the feasibility study of an entire-body PET scanner, especially in the sensitivity as well as count rate performance, as many of the evaluations performed on different devices has emphasized on this features. These two standards relate to the geometry of scanner directly, while other standards would also depend on other factor such as reconstruction algorithm. Additionally, these two were also what most of manufacturers usually refers when mentioning specification of any scanner device.

3.3. Sensitivity and Count Rate Performance

Two of the major characteristics of PET machine are the Sensitivity and Noise Equivalent Count Ratio (NECR) peak values. These features have a great contribution to the quality and detailed image of an object by the PET scanner, which is the major goal of PET studies. Therefore the performance of the scanner depends largely on these parameters to form a good quality image formation, which also include spatial resolution, noise, scattered radiations, and contrast. These parameters are interdependent, and if one parameter is improved, one or more of the other are compromised.

3.3.1. Sensitivity

Sensitivity is a function of the scintillation material, its thickness, the solid angle subtended by the detector array, and the scintillator packing fraction. The sensitivity is also defined as the ability to capture the number of counts per unit time detected by the device for each unit of activity present in a source [18]. Generally, the profile of axial sensitivity has a triangular shape. This value also depends on the detection efficiency, PHA window setting and dead time of the system [2,17, 30].

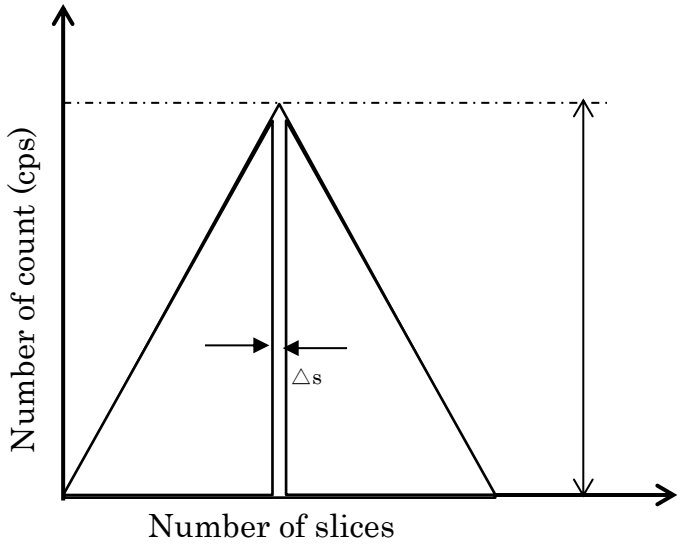

Figure 4 Axial Sensitivity Profile

There are other factors which also influence the sensitivity values such as stopping factor of the detector and the height of the crystal detectors and other recent development of detectors [19-21]. To limit the scope of the research, we have not involved these factors yet. However, we believe that with all these factors taken into account while developing entire-body PET, the sensitivity can be further improved.

3.3.2. Sensitivity and Solid Angle

Sensitivity is also depending on the solid angle, defined as the angle subtended by the source and the detector. If the distance between the detector and source is

increased, then the solid angle is decreased and so the sensitivity. This also mean, increasing ring diameter would also decrease sensitivity. On the other hand, increasing number of ring in the detector would increase sensitivity as the solid angle increased.

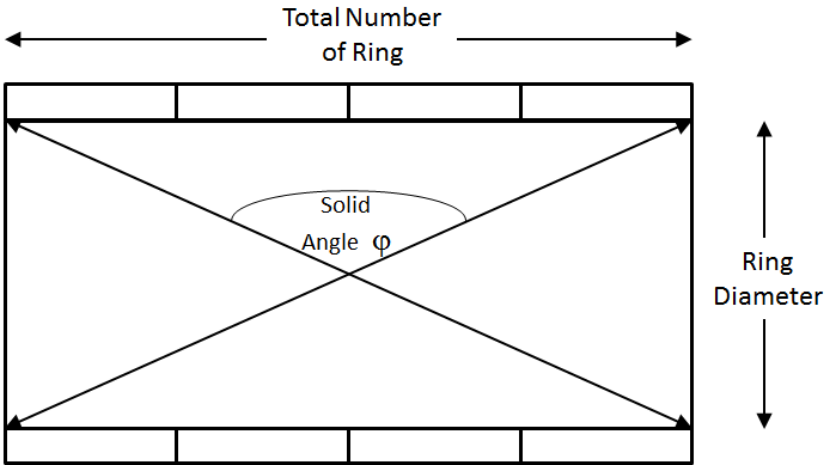

Figure 5 Solid Angle in a scanner and its relation to sensitivity

3.4. Count Rate Performance

Another main characteristic of PET is Noise Equivalent Count Rate (NECR) value. It determines the rate of true count in compare to the total count in the scanner geometry. This value is defined as:

$$\mathbf{NECR} = \frac{\boldsymbol{T^2}}{\boldsymbol{T + S + k\,R}} \qquad (1)$$

where *T*, *S* and *R* is True, scattered and random coincidence count respectively, and k =1 for conventional delayed windows, k=2 for real-time windows.

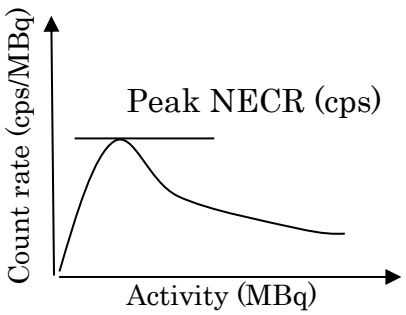

Figure 6 Noise Equivalent Count Rate (NECR) graph

By the extension of axial-FOV, the peak-value of NECR graph would be significantly improved. Obviously, the value of NECR can be improved by getting more counts. This can be achieved by longer acquisition period, injecting more radiopharmaceutical, or improving the detection efficiency of the scanner [5]. All these factors are limited by various conditions, for example too much activity cannot be administered because of increased radiation dose to the patient, random coincidence counts, and dead-time loss. Imaging for a longer period may be uncomfortable to the patient, especially those with clausthrophobia and improving the detection efficiency may be limited by the design of the imaging device. However, the value also depends on the scatter count rate in which an increase was introduced due to the extension of axial-FOV. Attenuation could also affect this value since the longer distance and material travelled by the photons to reach the detectors, the more probability that the energy would be attenuated.

3.5. jPET-D4 and DOI-Detectors

The geometry of PET scanner applied in this research is of jPET-D4 developed by National Institute of Radiological Sciences (NIRS), Japan [22-26]. It was designed as a dedicated brain scanning device, with a special feature of 4 layers depth-of-interaction (DOI) employed in the detectors. This scanner is designed to achieve not only high spatial resolution but also high sensitivity [24]. DOI information can minimize the effect of the crystal penetration of obliquely incident gamma rays.

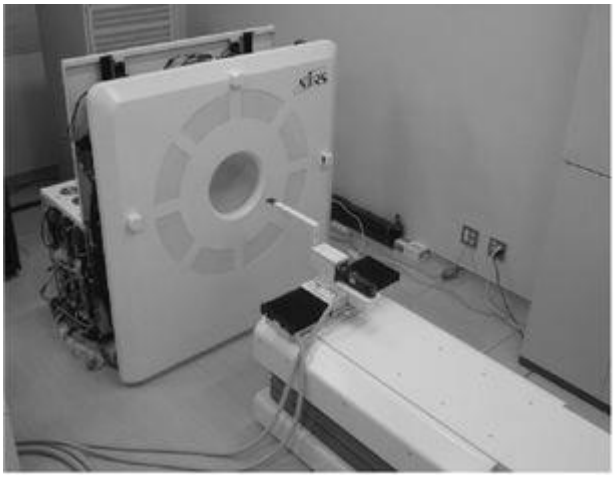

Figure 7 jPET-D4 developed by National Institute of Radiological Science (NIRS)

The major difference between ordinary PET and DOI-PET can be seen in Figure 8 . Using such detectors, we can derive DOI information in order to detect the location of the source more accurately. By employing several layers of crystal, this will maintain a high spatial resolution [27]. Our simulation model implements to the 4-layered DOI-PET scanner, but DOI information is not being used in this

simulation.

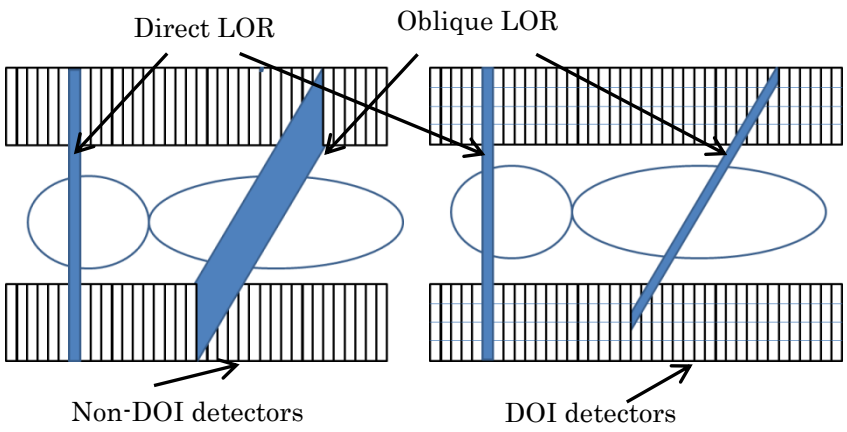

Figure 8 Differences between DOI and Non-DOI

3.6. Geant4 Application for Tomography Emission (GATE)

Geant4 application for tomography application (GATE) software is widely used in PET scanner simulation [28-30]. Our simulation are using GATE version 6.2 running on a 4 processor machine. This software can describe the geometry as well as physical process during an acquisition process of the defined scanner. This description is written in a macro file, which contain several steps :

- Defining Geometry and Material
- Defining Sources and Phantom
- Defining Physical Process
- Setting the output File and starting the acquisition
- Visualization

3.6.1. Defining PET Geometry and Material

The geometry of the PET is designed in such a manner that the crystal is made in 4 layers, which contains the depth-of-interaction (DOI) information. The crystal scintillator used is an Lutetium oxyorthosilicate (LSO) material which exhibits the reasonable fast scintillation decay time of all PET scintillators currently in use. Each crystal block was made of 16 x 16 array with dimension of 2.9 x 2.9 mm and thickness of 5 mm, coupled to a 52 mm square 256-channel flat panel PS-PMT (FP-PMT).

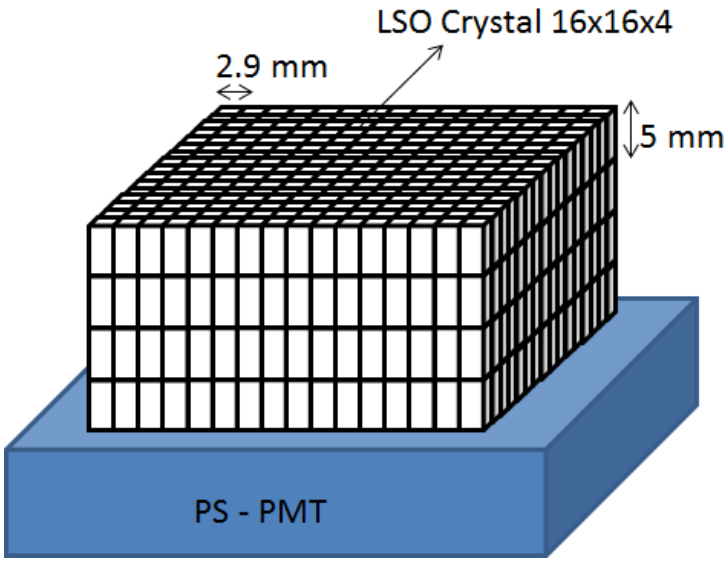

Figure 9 Detail of LSO Scintillation Crystal arranged in 16x16 array mounted on a PS-PMT

Every ring scanner comprises of several crystal block, depends on the type of ring diameter chosen in the design. For example, for 60 cm ring diameter, there could be 38 crystal blocks. Hence, for such ring scanner, there will be 38,912 crystals with volume of 42.05 mm^3 each. The axial FOV length of the standard scanner is

19.2 cm which consist of 4 rings of crystals block. This length could be extended according to the number of ring chosen in the design.

3.6.2. Source Definition

Radioactive sources should be defined during the simulation, in order to start the physical processes. The activity strength of the source itself is varied based on the test. For the sensitivity test for example, we are using the 50KBq sources, while other test might require sources up to 400 MBq.

Many activity distributions are available in GATE. At each new event, the source manager decides randomly which source decays, and generates for it one or more primary particles. As we are conducting a PET simulation, the back-to-back of gps particle type is employed with an energy of 511 keV. The volume and position of sources should also be described appropriately.

3.6.3. Defining Phantom

There are many different type of phantom material can be chosen from the PET library, for example water, air, polyehtylene and others. For the sensitivity test, no phantom is being used whereas the NECR test is using a Polyethylene material, with a cylinder shape. The size is the phantom is similar to that the NEMA NU2-2004, which is 20-cm in diameter but with an extended length of 175 cm to mimic the average size of human body.

3.6.4. Defining Physical Processes

Some standard physical processes are chosen from pre-defined list, such as Campton Scattering, Positron Annihilation and others. Once the program is initialized, the physical processes will also be started. This processed should be defined before the declaration of the sources.

3.6.5. Defining Acquisition Time, Output and Visualization

Having completed all the above setup, the simulation can be run and divided into several time slices. We should also defined the output file name, which will be saved in the form of a **root** file. Installation of Gate will include the installation of root software which can be used to analyze the result of the simulation and using an openGL, we can visualize the geometry of the scanner we developed as well as the physics processing occurring during simulation. Figure 10 shows some visual description of the scanner design using GATE software, for different axial FOV length.

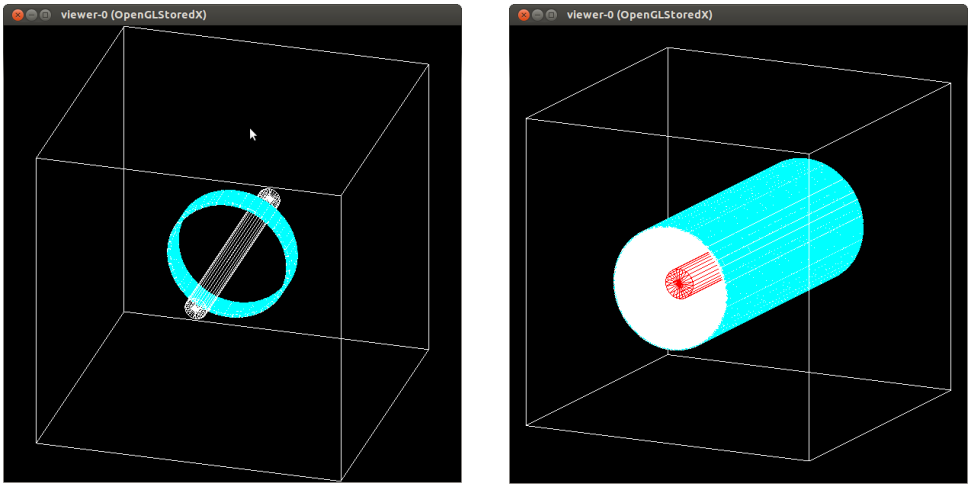

Figure 10 Visual representation of GATE software before any physical processes taken place

3.7. Preliminary Setting

Other than the geometry arrangement above, in order to get an optimum result of PET scanner simulation, few settings were to be done. These setting would affect the number of count achieved during the simulation. There are other parameter other than these mentioned below, but these are those parameter which would affect most to the performance of the PET scanner.

3.7.1. Windows Energy Setting

Window Energy is an interval of energy limit in which a pair of events are still considered a true coincidences, it they were within this limit, otherwise they will be rejected. This value can be set in to that the number of counts received, reach its optimum. Figure 11 shown that at energy level 450-600 keV, the performance of PET scanner for this particular design, reach its optimum.

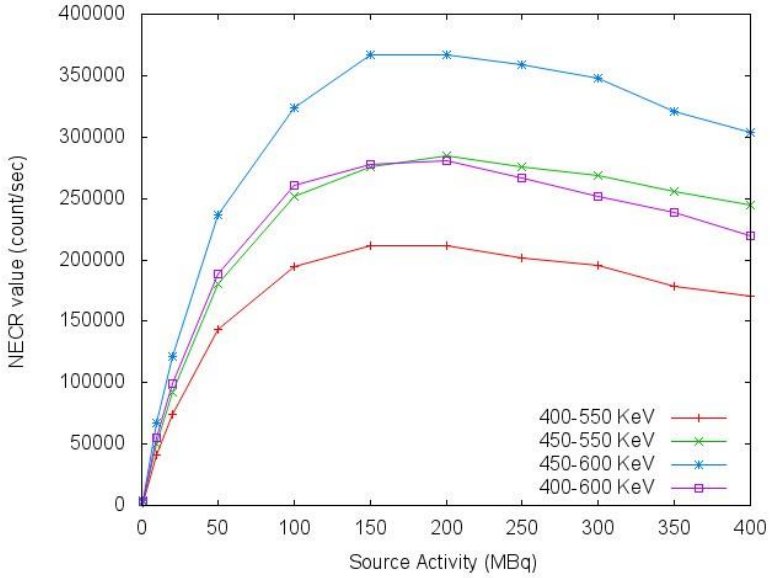

Figure 11 Energy Window setting to achieve optimum NECR values

3.7.2. Coincidence Windows

Coincidence windows are a time window in which two single events would be regarded as a coincidence count, if they were detected in a detector pair within this coincidence window frame. Bigger coincidence window might result in many true count, but at the same time, it also lead to additional random and scatter count. Some simulations were conducted to get the optimum result on true count

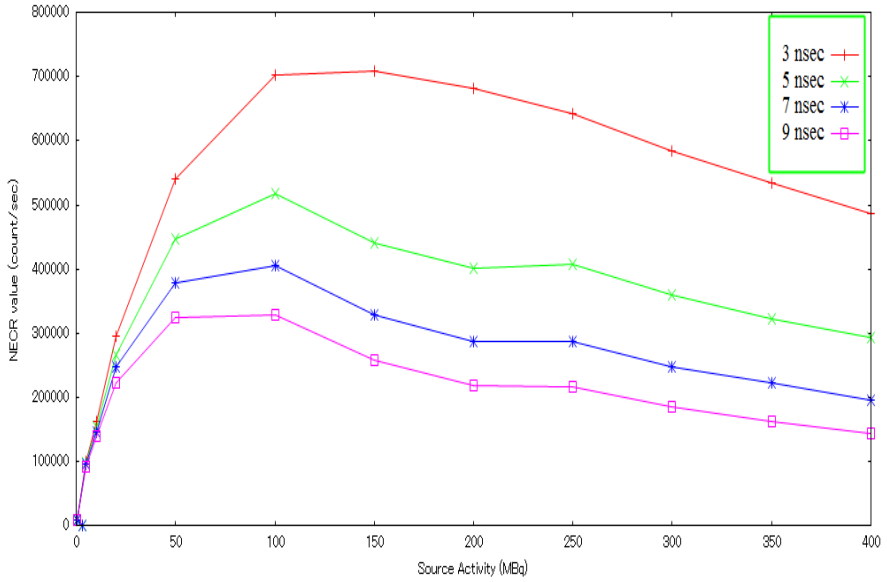

Figure 12 Coincidence time window selection for the best NECR peak values

From the above graph we can see than the NECR has its highest peak at 3 nsec. Note that for PET, coincidence time windows denote 2τ but, in the GATE program this values is set to τ. Hence by defining 3ns in the GATE program for example, is actually 6ns in reality.

3.7.3. Timing Resolution

The time resolution of a detector is usually defined as the minimum time interval between two subsequent photon events in order for these to be recorded as separate events [7]. We varied the time simulation between 0.6 up to 2 nsec, in 3 different PET geometry and observe its effect to the NECR values. Fig. 10 shows that there is no significant change in terms of NECR as we change the timing

resolution. Hence, we will set the time resolution to be 1.4 ns, which is suitable for LSO scintillators.

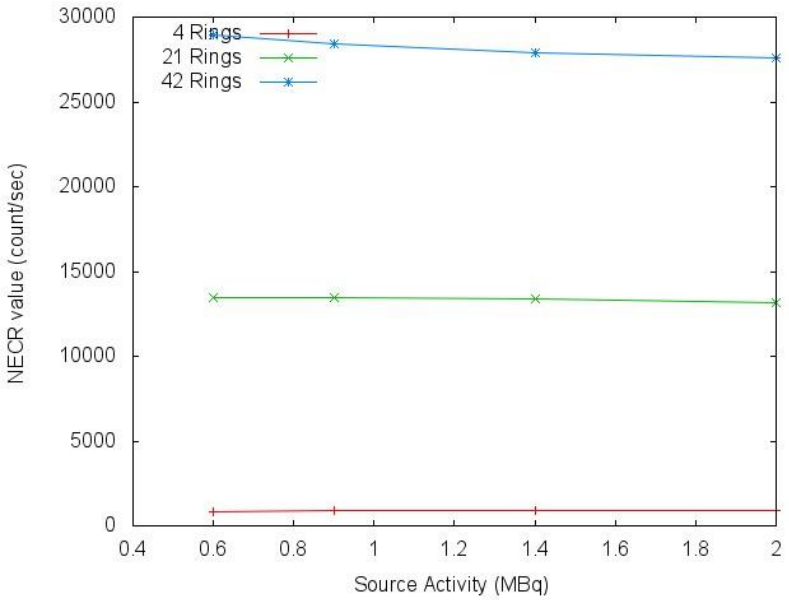

Figure 13 Time resolution versus NECR values

3.7.4. Dead Time

When a 511-keV photon interacts within the detector and is absorbed in the crystal, light photons are produced, which strike the photocathode of the PM tube. A pulse is generated at the end of the PM tube and amplified by an amplifier; the energy and the spatial position of the photon are determined and finally a count is recorded. When two such events are detected by two detectors in the time window, a coincidence event is recorded. [7,17]

The total time required to complete the above steps is defined as the *dead time* (τ) and is related to the signal integration time that depends on the electronics

and the scintillation decay time. During this time the detection system is unable to process a second event, which will be lost. This loss (called the dead-time loss) is a serious problem at high count rates and varies with different PET systems. It is obvious that the dead-time loss can be reduced by using detectors with shorter scintillation decay time and faster electronics in the PET scanners.

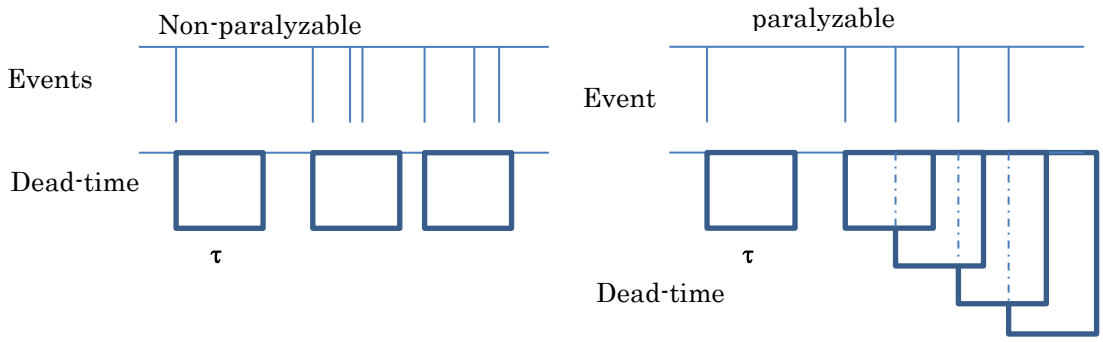

Figure 14 Two types of dead-time: Non-paralyzable (left) and paralyazable (right)

Dead-time system is very much related to the efficiency of the detectors. There are two fundamental types of dead-time applied in to the detectors of the scanner, namely the non-paralyzed and paralyzed dead-time as shown in Figure 14. The first one will ignore any incoming events during the dead-time period, and it will become active after a period of τ. While the paralyzed case, the coming of another event during a dead-time will extend the dead-time period starting from the time of arrival of such event. Hence, for big number of events, this dead-time might cause pile up and even it might reach a stage that no other events will be accepted. Thus the system is paralyzed.

In our system, a paralyzed dead-time is applied for individual detectors with a dead-time of 250 ns, while for grouping axially stacked detectors, a non-paralyzed

dead-time of 256 ns is applied. Due to current design of PET scanner, the first dead-time is still unavoidable, while the grouping dead-time can be managed by few methods such as choosing a smaller dead-time value or making a smaller grouping of detectors

3.7.5. Coincidence Sorter

There are few coincidence sorter policy which can be applied such as *TakeAllGoods, TakeIfGoods, TakeWinnerOfGoods, RejectAllGoods* etc. In our experiment we are applying *TakeWinnerOfGoods* in which among the true coincidences detected, we only choose a pair with the maximum energy, and discard others. Take-all-goods policy yields higher count rates compared to the Reject-all-goods policy. Take-all-goods under estimate the random rate and the Reject-all-multiples over estimate the random, which results overestimation with Take-all-goods and underestimation with Reject-all-multiples in NECR calculation. The discrepancy is more significant for smaller phantoms. [32]

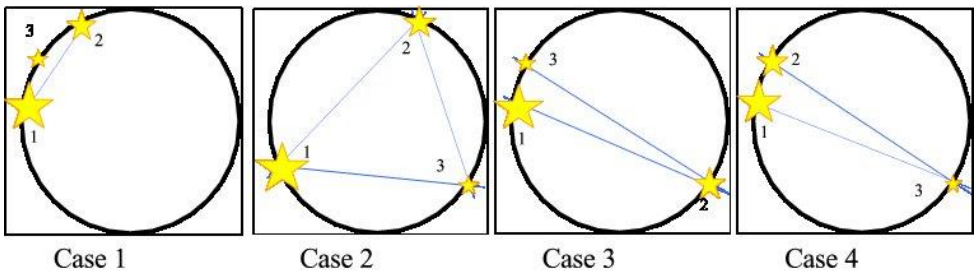

Figure 15 Multiple Coincidence Sorter Policy. With TakeWinnerOfGoods, in case1,2 and 3, pair 1 and 2 will be chosen, while in case 4, pair 1 and 3 is selected

3.7.6. Summary

Below is the flow of the process during the simulation of an entire-body PET using a GATE software, until it produces the axial sensitivity profile and count rate performance curve. These parameters has to be chosen properly, in order to show the optimum performance of the scanner. The GATE software would simulate the near to real situation during the simulation, however we have not deal with error corrections during the calculation of the sensitivity and NECR values.

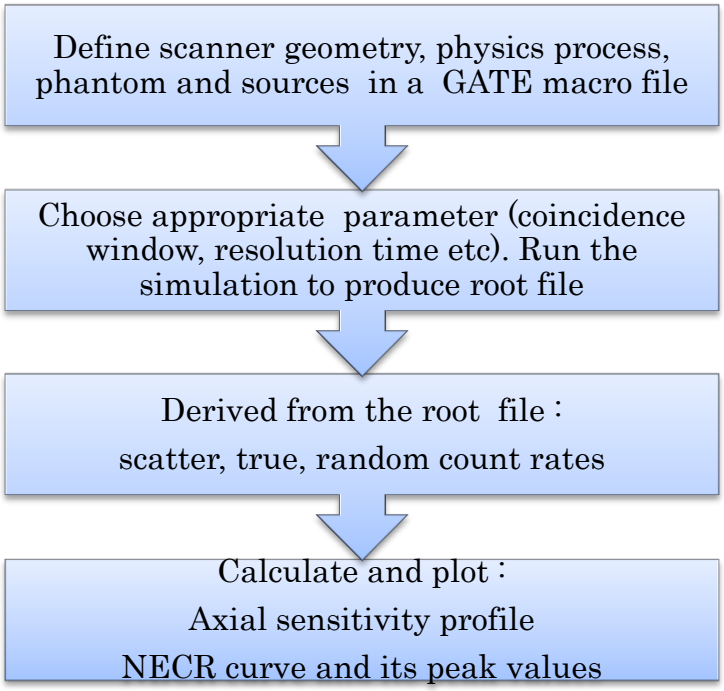

Figure 16 Flowchart of the sensitivity and/or NECR simulation test

Chapter 4

Monte-Carlo Simulation of Entire-body PET

4.1. Background

Axially extended FOV PET scanner was expected to have higher sensitivity [1,2] compared to the conventional one. Studied has shown with the increase of axial FOV, sensitivity has increased. Nevertheless, cost has been the main drawback of entire-body PET scanner, besides of other factor. Hence, the first part of this experiment is to show the increase of sensitivity and peak value of NECR for entire-body PET scanner with standard diameter. For the sake of cost saving, in the second part of the experiment, we then use a smaller diameter and compare its performance with the standard diameter.

4.2. Simulation Setup

The scanner geometry used in this experiment is as described in chapter 3. There will be 3 types of scanner in terms of its length. The first geometry is the standard or conventional PET scanner, with the axial FOV of 20 cm or equal to 4 rings. The other 2 geometries are the axially extended scanner, which will be extended up to 100 cm or equal to 21 rings, and 200 cm or equal to 42 rings as shown in Figure 17. In the first part of the simulation, we use an 80 cm diameter scanner. Detail specification can be seen in table 1.

Table 1 Detail Specification of Scanner with different axial FOV

Crystal size	2.9 x 2.9 x 5 mm
Crystal material	LSO
Number of crystals	16 x 16 x 4 (per detector)
Number of detector rings	4 = 19.2 cm 21 = 100.8 cm 42 = 201.6 cm
Ring diameter	60 and 80 cm
Timing resolution	1.4 ns
Coincidence time window	6 ns
Energy resolution	15 %
Energy window	450-600 keV
Dead-time grouping	Non-paralysable : 256 ns
Dead-time individual	Paralysable: 250 ns
Coincidence Sorter	TakeWinnerOfGood

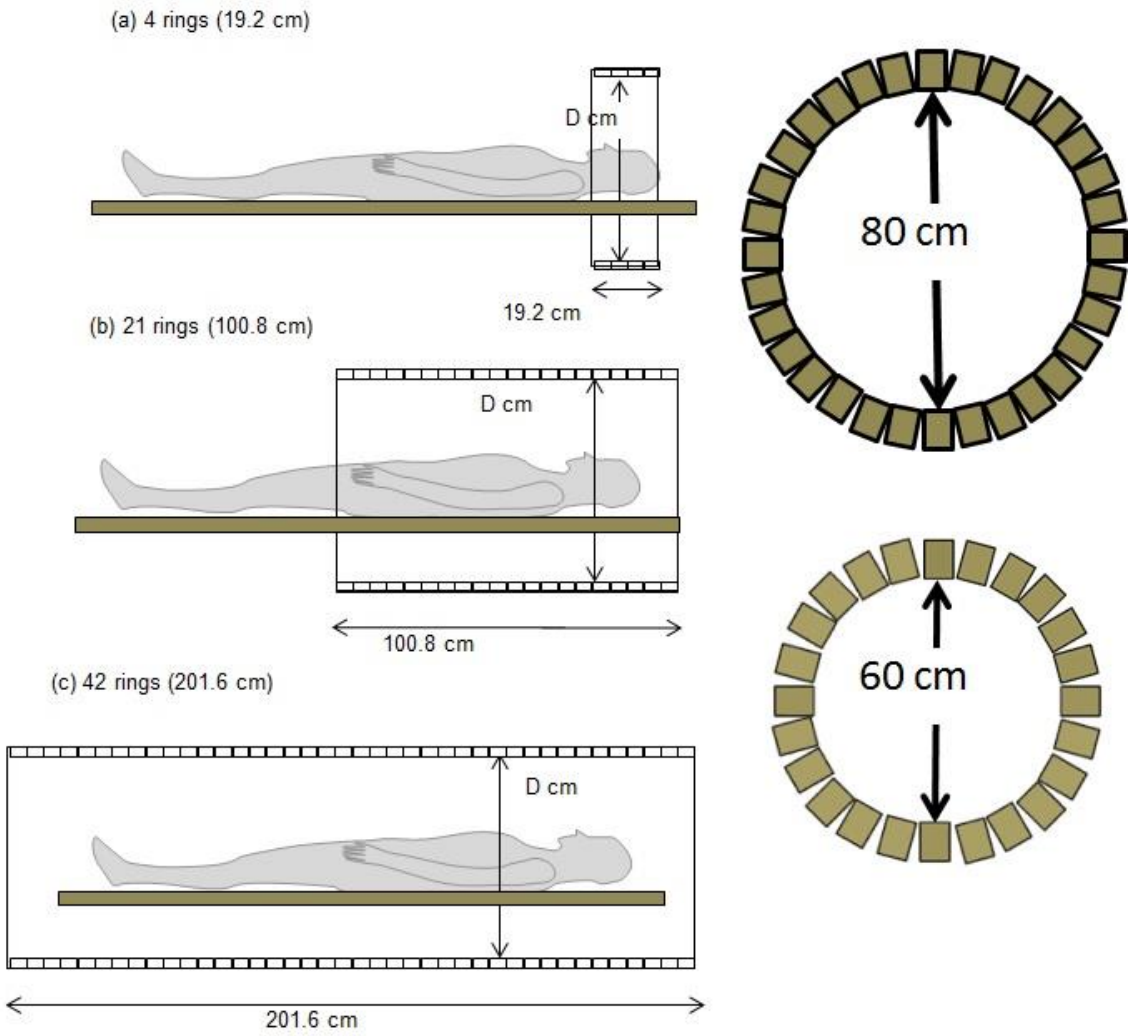

Figure 17 Scanner design with different axial FOV and diameter

The performance of all the scanner geometry will be based on the two tests of sensitivity and count rate as described in the previous chapter.

4.2.1. Sensitivity Test

In order to conduct the sensitivity test, a 175-cm line source of 50 kBq, an average

height of human body, was used in the simulation and the relative sensitivity for the six types of PET scanners was measured. These sources were set in the center of the FOV. The number of detected true coincidences was computed and system sensitivity profiles with single bed position were calculated using the line source. Each measurement time was 1200 s. The conventional scanner with 20 cm FOV length, would have to take several bed-step when scanning whole-body images. Hence, for the same total amount of time, time taken per bed-step will be much lower. Our experiments are using 1200 seconds total acquisition time for all type of scanner, hence for every bed-step the amount of time taken is shown in the table 2. Total axial FOVs and measurement times for each situation were 201.8 cm and 1200 s, respectively.

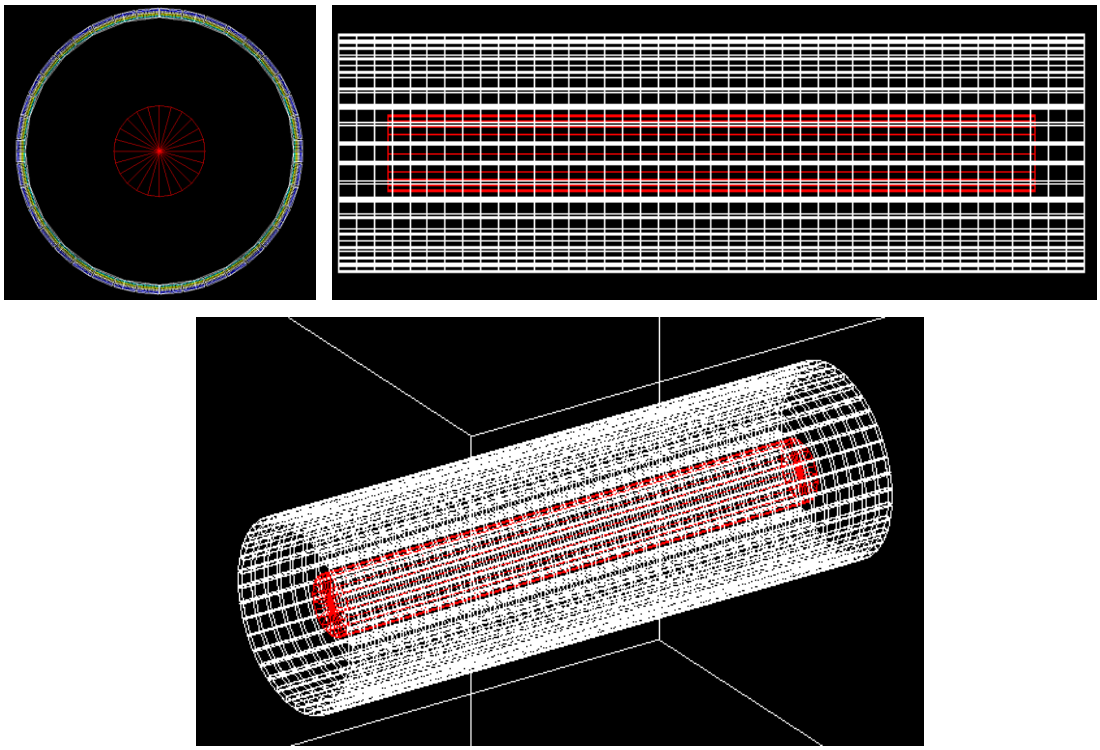

Figure 18 GATE visualization of entire-body PET scanner with 42 ring (white) nd 175 cm phantom (red) of 20 cm diameter at different view.

Table 2 Time taken for each bed step acqusition for same total scanning time for different scanner geometry

Number of Ring	Scanner Length	Number of bed-step	Acquisition time per bed
4 Ring	20 cm	19 bed	62 sec
21 Ring	100 cm	3 beds	361 sec
42 Ring	200 cm	1 beds	1200 sec

4.2.2.Sensitivity of Single-bed Acquisition

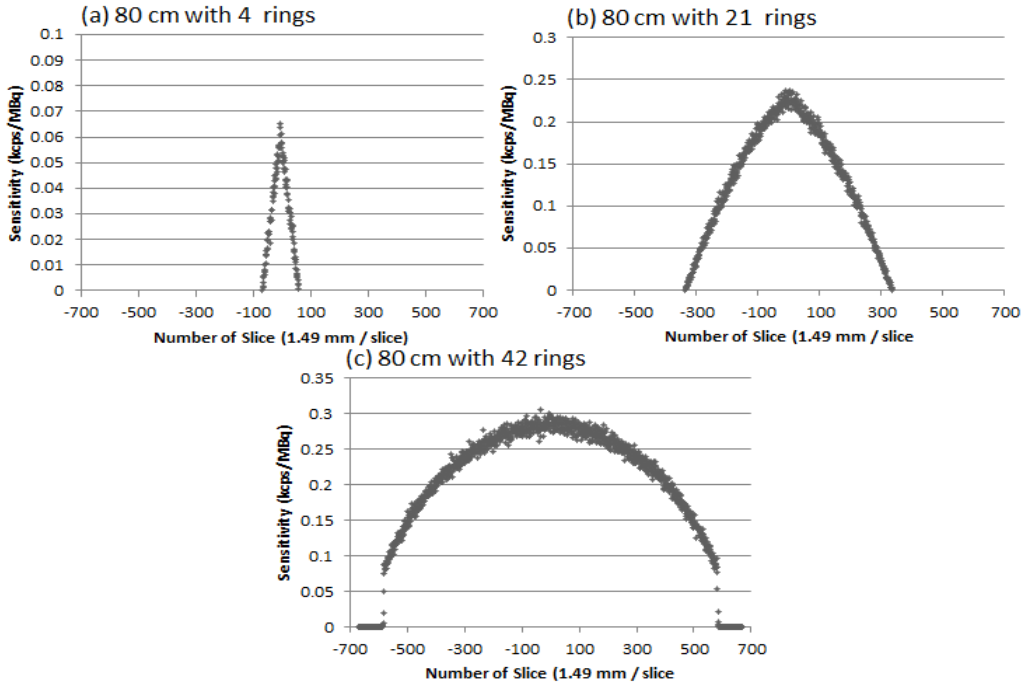

Figure 19 Axial Sensitivity Profile for single bed acquisition

Figure 19 shows the axial sensitivity gain in the case of single-bed acquisition, in which it was conducted in one position. In other words, the total sensitivity gain achieved was 4.77 in comparison between entire-body and conventional PET scanner as described in Table 3.

Table 3 Sensitivity gain for 3 different scanner with 80 cm ring diameter with single-bed acquisition

Sensitivity (Kcps/MBq) and its gain in parentheses	
Number of Ring	80 cm diameter
4	68.79 (1)
21	261.49 (3.8)
42	328.13 (4.77)

4.2.3. Sensitivity of Multiple-bed Acquisition

Acquisition was also conducted on different number of bed as mentioned before, with total acquisition time of 1200 sec. Figure 20 shows the significant increase on sensitivity for different axial FOV. A gain of 68.0 is achieved for entire-body PET when compared to conventional one, as seen in table 4.

Table 4 sensitivity gain for multi-bed acquisition

Number of Ring	Sensitivity in kcps/MBq (gain in bracket)
4 rings	3.84 (1)
21 rings	89.0 (23.21)
42 rings	260.8 (68.00)

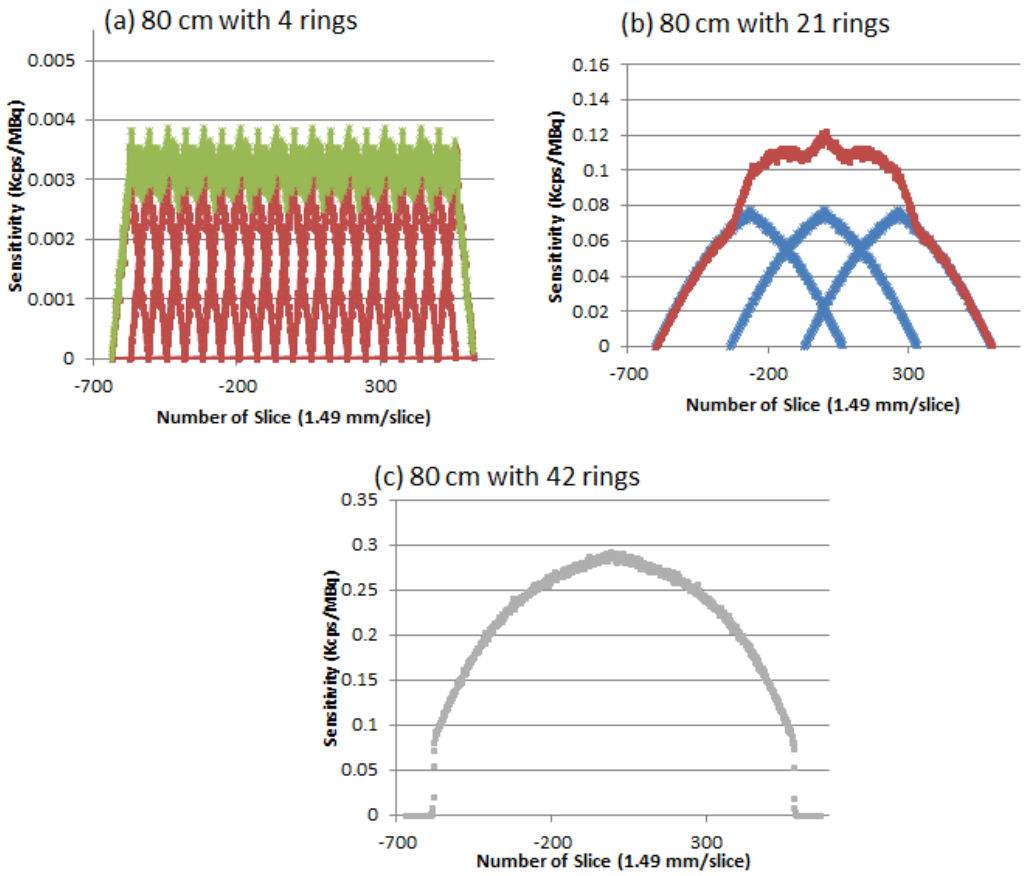

Figure 20 Sensitivity Profile for multi-bed acquisition with 80 cm ring scanner and 3 different scanner length

4.2.4. Shape of Sensitivity

If we observe the shape of sensitivity as the FOV gets longer, it becomes an distorted triangle. As sensitivity has a direct relationship with the acceptance angle, and as the axial FOV is getting bigger, the acceptance angle is also getting bigger and at one point it gets saturated. Hence, the shape of the sensitivity profile is no longer perfect triangular at long scanner, but it is more flat on the middle part of the scanner.

4.2.5. NECR

The count rate performance of a scanner is represented by its NECR graph. The peak value of NECR shows the optimum activity in which the scanner will perform efficiently. The test utilized a solid polyethylene cylinder phantom (175 cm long and 20 cm in diameter) with the 175 cm source centered of FOV. The phantom was modified on the NEMA NU-2 2001 standard. Source activity was varied from 0.5 up to 400 MBq.

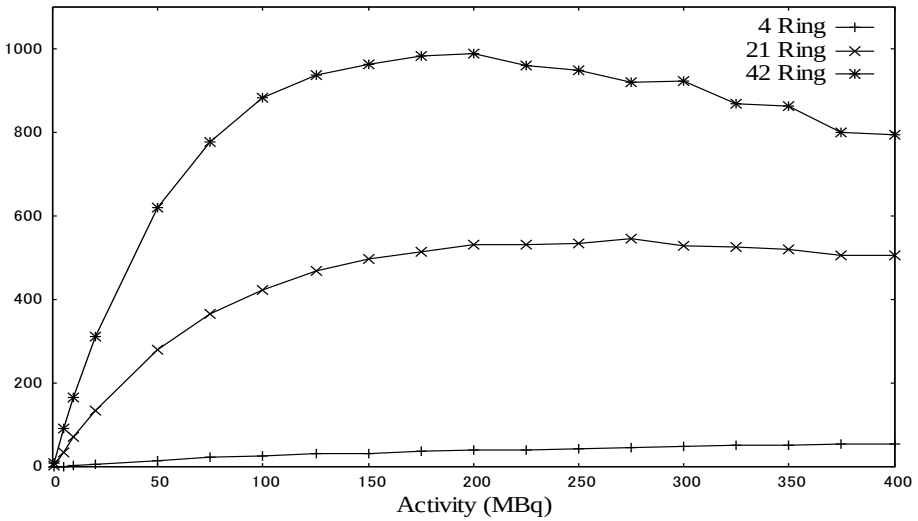

Figure 21 NECR graph for 80 cm diameter with 3 different scanner length

Figure 21 and Table 5 shows the dramatic increase in terms of NECR peak value for entire-body PET, more than 18 times in comparison to conventional one.

Table 5 NECR peak values of 80 cm ring diameter scanner and its gain for 3 different FOV length in parentheses

NECR peak values in kcps	
Number of Rings	80-cm diameter
4	55.1 (1)
21	546.1 (9.9)
42	989.1 (17.95)

4.3. Smaller Scanner Axially Extended PET

The main drawback of such system is still a high production cost due to large number of crystals required. There was also a study which replaced the scintillator detector material with cheaper Resistive Plate Chamber (RPT), yet the efficiency of such detector is pretty low for low energy [3]. Hence, we studied a smaller diameter entire-body DOI-PET (60 cm diameter) which we thought to be a cost saving and at the same time maintaining its sensitivity value.

4.3.1.Sensitivity

4.3.1.1. Single-bed Acquisition

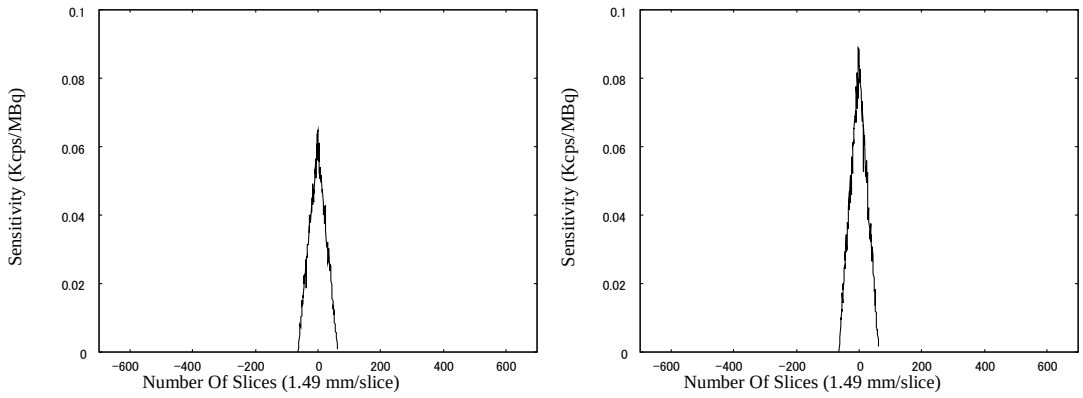

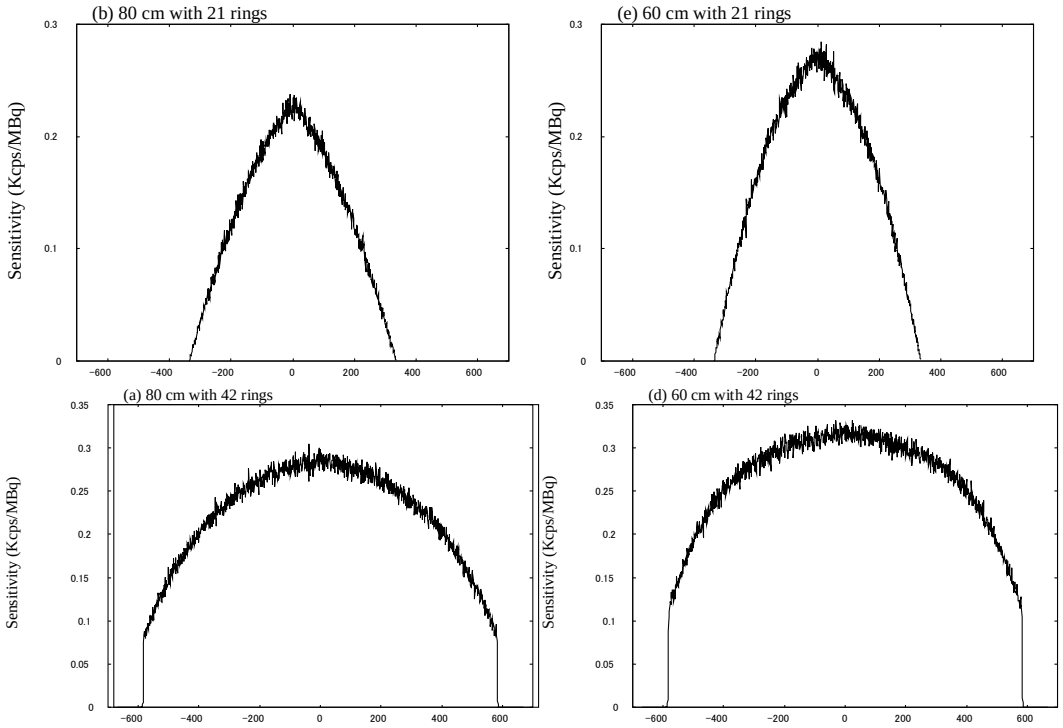

Figure 22 Axial sensitivity profile comparison between 60 and 80 ring diameters for single-bed acquisition.

Figure 22 shows the axial sensitivity profile for single bed acquisition for these 6 different types of scanner. As we can observe, for entire-body PET, in the mid-slice there was an increase of sensitivity around 15 % for 60 cm diameters. The total sensitivity for smaller scanner is in fact now 5.33 times better than conventional scanner as stated in Table 6.

Table 6 Sensitivity gain comparison between 60 and 80 cm ring diameter PET scanner for single-bed acquisition

Number of rings	Sensitivity (kcps/MBq)	
	60 cm diameter	80 cm diameter
4	95.04 (1.38)	68.79 (1)
21	314.91 (4.58)	261.49 (3.8)
42	366.94 (5.33)	328.13 (4.77)

4.3.1.2. Multi-bed Acquisition

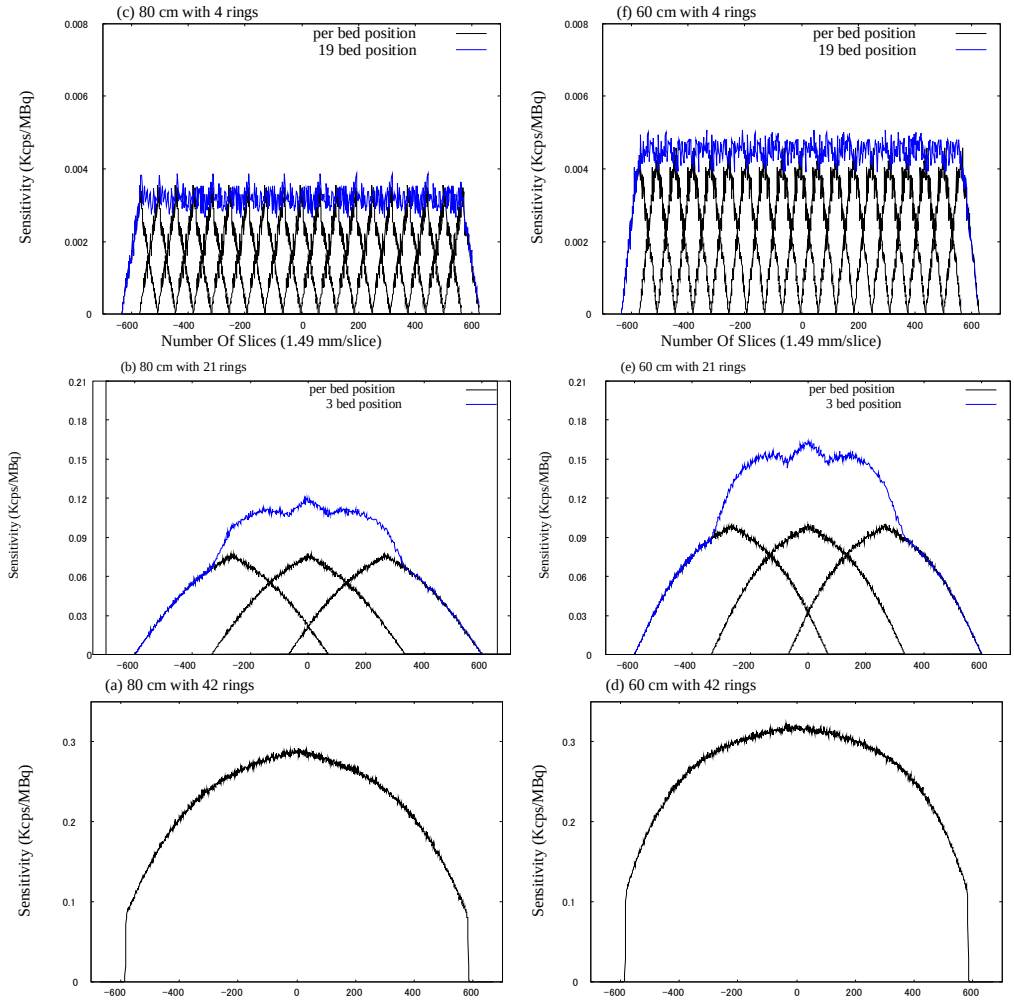

Figure 23 Axial Sensitivity Profile comparison between 60 and 80 ring diameters for multiple-bed acquisition

In terms of multi-bed acquisition, smaller scanner entire-body PET also performed better than the 80 cm diameter scanner. The total sensitivity gain is now 80 times compared to 68 times for the 80 cm diameter scanner, as shown in Figure 23 and Table 7.

Table 7 Volume Sensitivity (gain in parentheses) comparison between 60 and 80 cm ring diameter PET scanner for multiple-bed acquisition

Axial FOV(cm)	Sensitivity (kcps/MBq)	
	60 cm diameter	80 cm diameter
19.2	5.67 (1.48)	3.84 (1)
100.8	122.67 (31.98)	89.0(23.21)
201.6	306.73 (79.97)	260.8 (68.00)

4.3.2. NECR

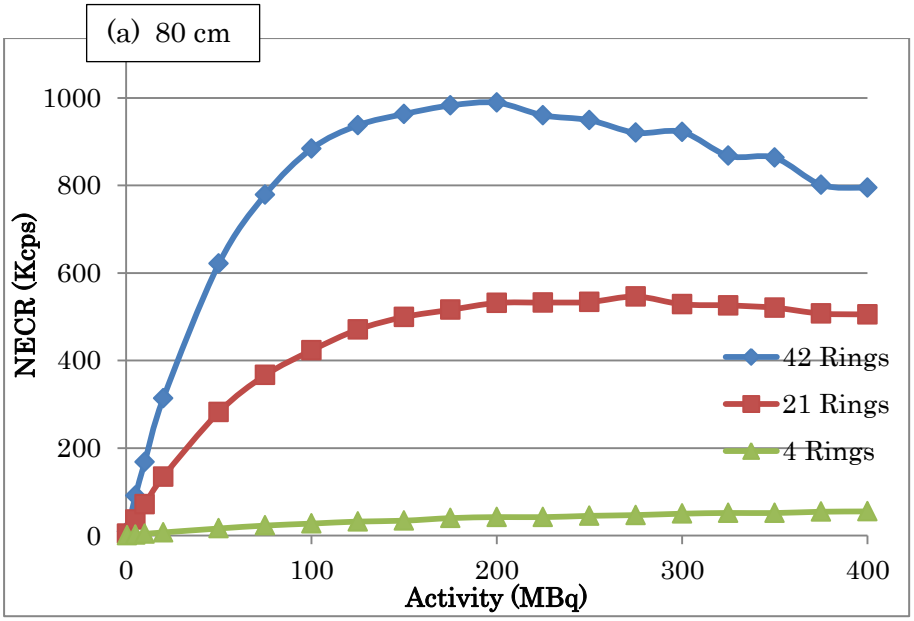

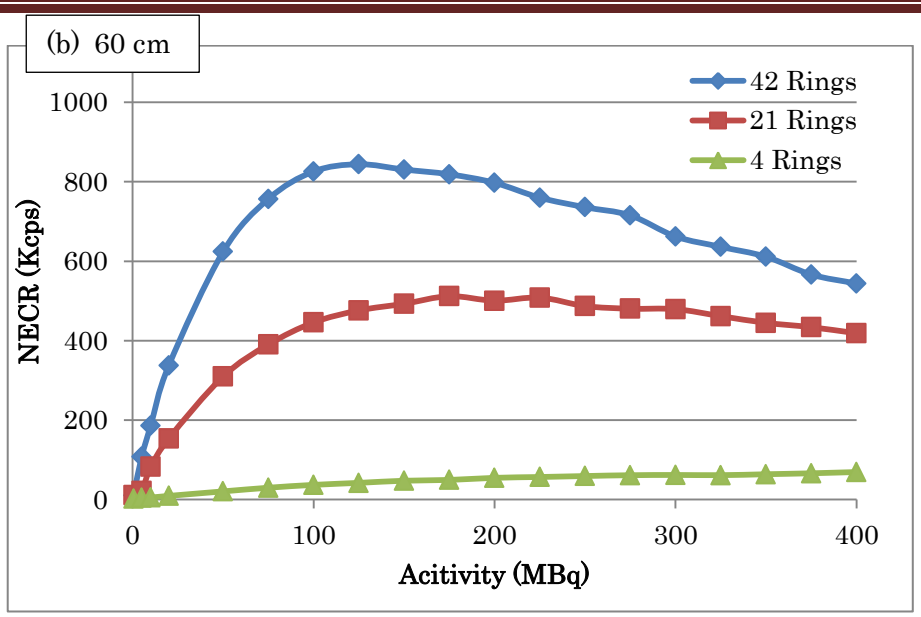

Figure 24 NECR graphs for 80 cm and 60 cm ring diameter scanner for 3 different axial FOV.

Figure 24 shows the graph of NECR value for 3 different axial FOV scanner, with different diameter. The top graph is the performance of PET scanner with 80 cm diameter while the bottom was the smaller 60 cm diameter PET.

Table 8 NECR Gain for Different PET Scanner in comparison to conventional scanner.

Number of rings	Peak NECR (kcps)	
	60-cm diameter	80-cm diameter
4	69.4 (1.25)	55.1 (1)
21	511.9 (9.29)	546.1 (9.9)
42	843.9 (15.31)	989.1 (17.95)

From the table and graph, for the entire-body PET, the 80 cm ring diameter achieved a higher NECR peak values by 17%.

4.4. Maximum Ring Difference (MRD)

Figure 25 shows that by choosing different maximum ring difference (MRD), the NECR values achieved could be optimize. As NECR depended on true as well as random and scatter events, the limitation of ring difference would affect the number of count for each of these events. As entire-body PET means introducing many more oblique LORs, hence it will induce more scatter as well as random counts. By limiting the process to a certain MRD, it will minimize these counts, and hence, to a certain limit the NECR values were improved. These will also mean reduction of data size need to be managed for image reconstruction.

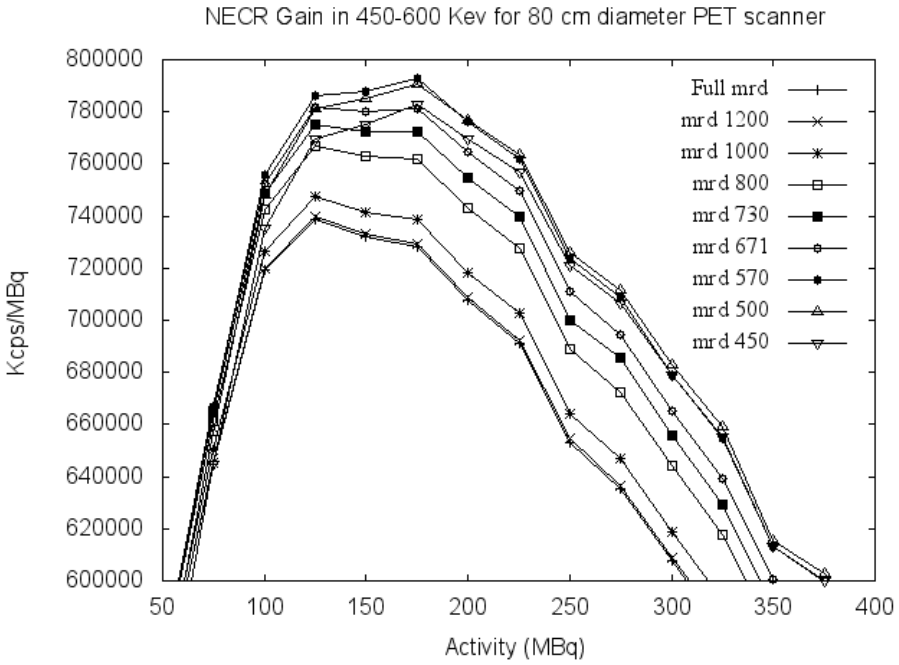

Figure 25 The effect of mrd choice to the value of NECR

4.5. Summary

The entire-body PET is promising a high sensitivity and NECR peak values. A gain of sensitivity up to 80 times can be achieved if the diameter of the scanner is made smaller to 60 cm. This smaller scanner has sensitivity 15% higher than the larger scanner. However, the NECR peak value for smaller diameter is not as high as the standard 80 cm diameters. While the 80 cm diameter scanner achieved a gain up to 18 times compared to conventional scanner, 60-cm scanner is only having a gain of 15. However, even with these values, the entire-body PET could potentially reduce the scanning time per patient dramatically or minimize the dose injected during treatment, which is a great contribution for PET imaging.

Chapter 5

Evaluation of Entire-body PET with Several Ring Diameters

5.1. Background

Having the result for NECR peak values for entire-body PET, for both 60 and 80 cm ring diameter scanner, it is interesting to find out more about these characteristics for other diameter or other length as well. Despite of higher sensitivity, the peak value of NECR for the 60-cm ring diameter was less than that of 80-cm ring diameter scanner. We deduce that this phenomenon is the result of single data loss for grouping axially stacked detectors using the conventional DAQ architecture. In the 2-m long PET scanner with the conventional DAQ architecture, single data throughput was saturated in limited activity. As a result, single data loss at the grouping circuits were limited to the peak NECR for the

entire-body PET scanner.

5.2. Experiment Setup

In this part, we introduced two more scanner ring diameter namely 70 and 90-cm, being smaller and larger than the standard diameter. At the same time, an additional extended axial-FOV of 30 ring was also introduced which is equal to 144 cm long as seen in Figure 26 and Figure **27**.

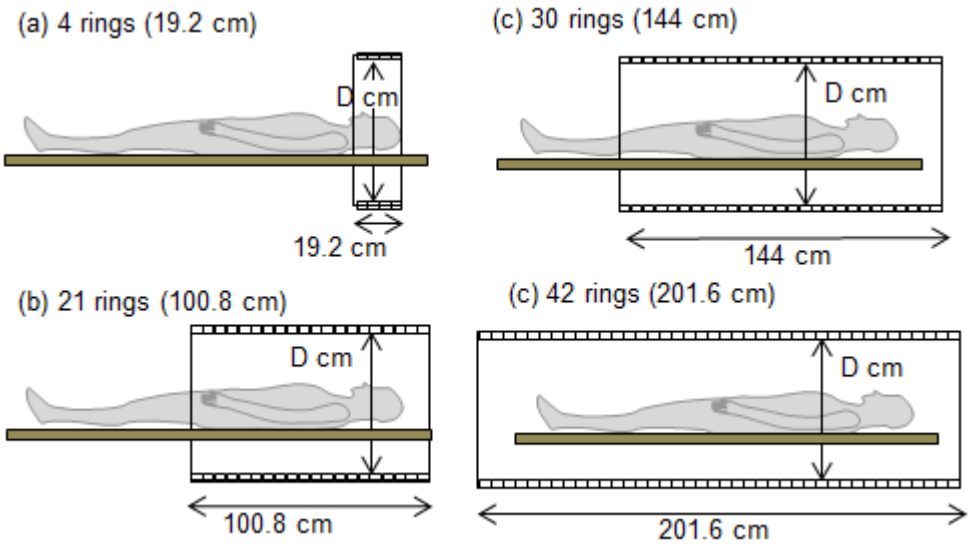

Figure 26 Scanners with 4 different axial-FOV length, will be combined with 4 different ring diameters

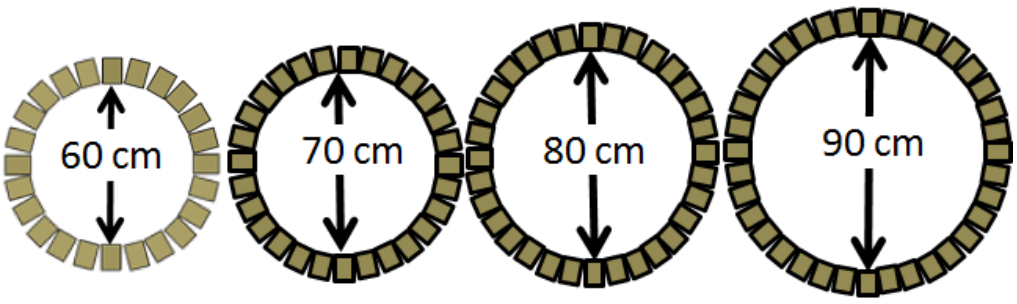

Figure 27 illustration of different scanner ring diameter and its crystal arrangement

Table 9 Specifications of Scanner with 4 different ring diameter

Crystal size	2.9 x 2.9 x 5 mm
Crystal material	LSO
Number of crystals	16 x 16 x 4 (per detector)
Number of detector rings	4 = 19.2 cm 30=144.0 cm 21 = 100.8 cm 42 = 201.6 cm
Ring diameter	60, 70, 80, 90 cm
Timing resolution	1.4 ns
Coincidence time window	6 ns
Energy resolution	15 %
Energy window	450-600 keV
Grouping Dead-time	Non-paralysable : 256 ns
Integrated Dead-time	Paralysable: 250 ns

We also tried to optimize the number of crystal in every crystal block, by minimizing the gap between each block. Nevertheless, due to geometry constraint, the gaps between different ring diameters cannot be equal as shown in Table 10 .

Table 10 Gaps between crystal block for different scanner ring diameter

	60 cm	70 cm	80 cm	90 cm
Number of crystal block per ring	38	44	50	56
Circle circumference (cm)	188.50	219.91	251.33	282.74
Number of Crystal per ring	2490368	2883584	3276800	3670016
Crystal Volume per ring (litre)	41.89	48.50	55.12	61.73
Gap between Crystal block (cm)	0.16	0.20	0.23	0.25

5.3. Sensitivity Test and NECR

The same procedure for Sensitivity and NECR test as described in chapter 3 is also applied in this experiment. In addition, we also measure the dead-time loss due to grouping dead-time, by comparing the result with and without grouping dead-time. Acquisition time in this case is 120 sec for all type of scanner

geometry.

5.3.1.Sensitivity Results

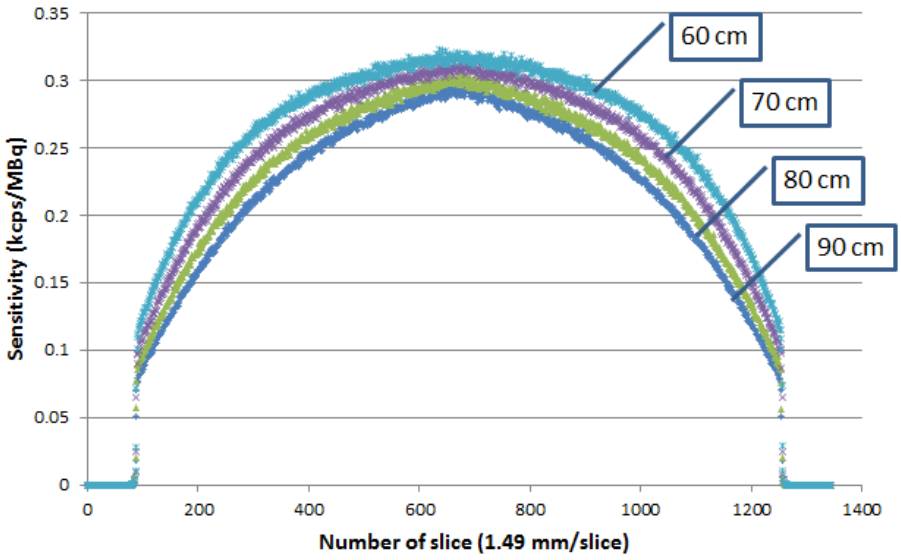

Figure 28 Sensitivities of Entire-body PET scanner with different ring diameter

Figure 28 shows that the true sensitivity of each scanner diameter is increasing as the diameter getting smaller, for the case of entire-body PET. This result is consistent with the fact that as the diameter getting smaller, solid angle has become larger, and therefore it increases the sensitivity.

Table 11 describes that the increase of volume sensitivity which can be as high as 75 times in comparison to conventional PET scanner. Which also mean, for entire-body PET, smaller scanner can achieve sensitivity 12.5 % higher than 80 cm diameter scanner.

Table 11 Volume Sensitivity in kcps/MBq for axially extended DOI-PET and its gain (in bracket) in comparison to conventional scanner 20cm long 80 cm diameter

	Scanner diameter			
	90 cm	80 cm	70 cm	60 cm
42 ring	257.96 (62.65)	272.76 (66.25)	289.05 (70.20)	306.73 (74.49)
30 ring	156.93 (38.11)	169.13 (41.08)	182.22 (44.25)	197.38 (47.94)
21ring	86.20 (20.94)	94.00 (22.83)	103.22 (25.07)	114.49 (27.81)
4 ring	3.60 (0.87)	4.12 (1.00)	4.67 (1.13)	5.37 (1.30)

5.3.2. Single Count With Dead-time Loss

Single data is produced during the physical process of GATE simulation in abundant number. Two pair of singles was classified based on the coincidence sorter policy within the coincidence time window, to form a coincidence pair, which is either true, random or scatter coincidence event. While not every singles will make these pairs due to the fact that their occurrence might not fall within the coincidence window, or were not considered as a coincidence pair based on the coincidence sorter policy, many of them were also lost due to some sorting mechanism. While there are many pairs of ring need to be sorted at a particular time, the machine will not be able to handle all these pairs at a very incredible fast time. Therefore, a dead-time period is set, in order the machine to process the next coming pairs to be sorted. Hence during this dead-time period, the machine will

not be able to sort out any other pairs, even though they might be a true coincidence. This is called the dead-time loss.

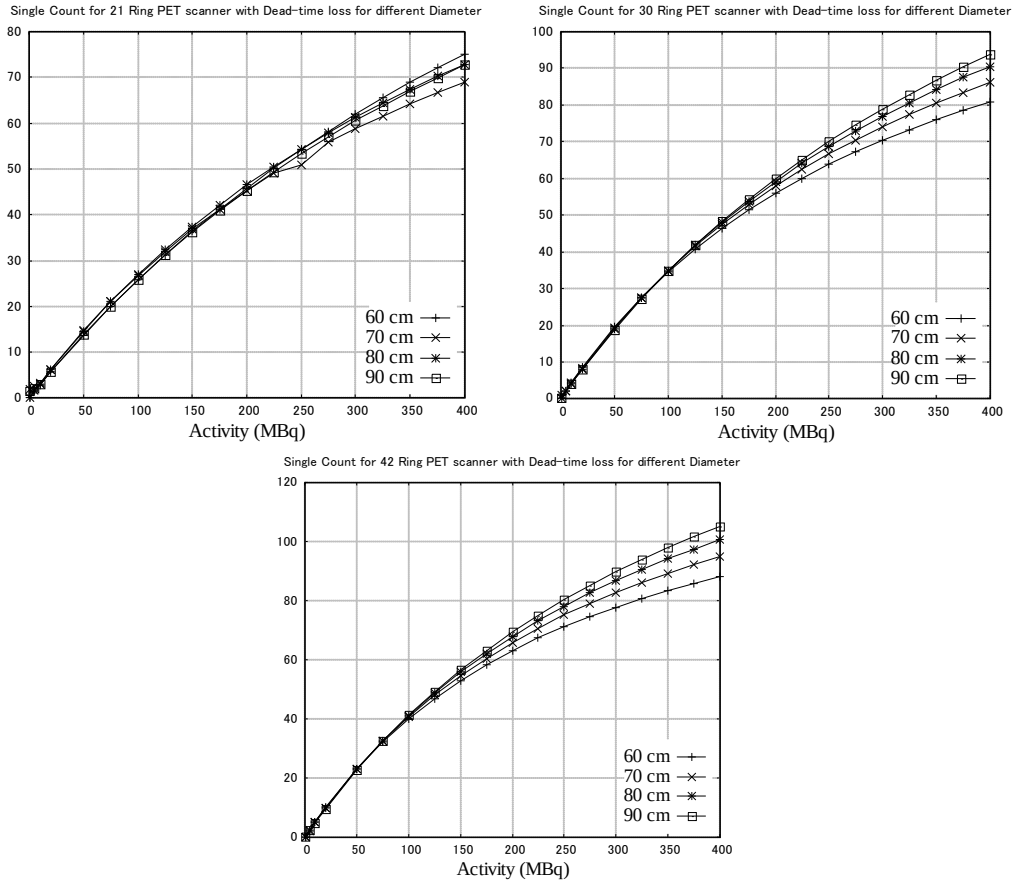

Figure 29 Single count of 3 different Axial-FOV PET scanner with both integration and grouping dead-time applied

This can be explained in Figure 29 in which single-count graph for every scanner with different diameter. Naturally, scanner with smaller diameter would have a higher number of single-count. But it is shown that the single count for larger diameter has a higher count for axially extended FOV.

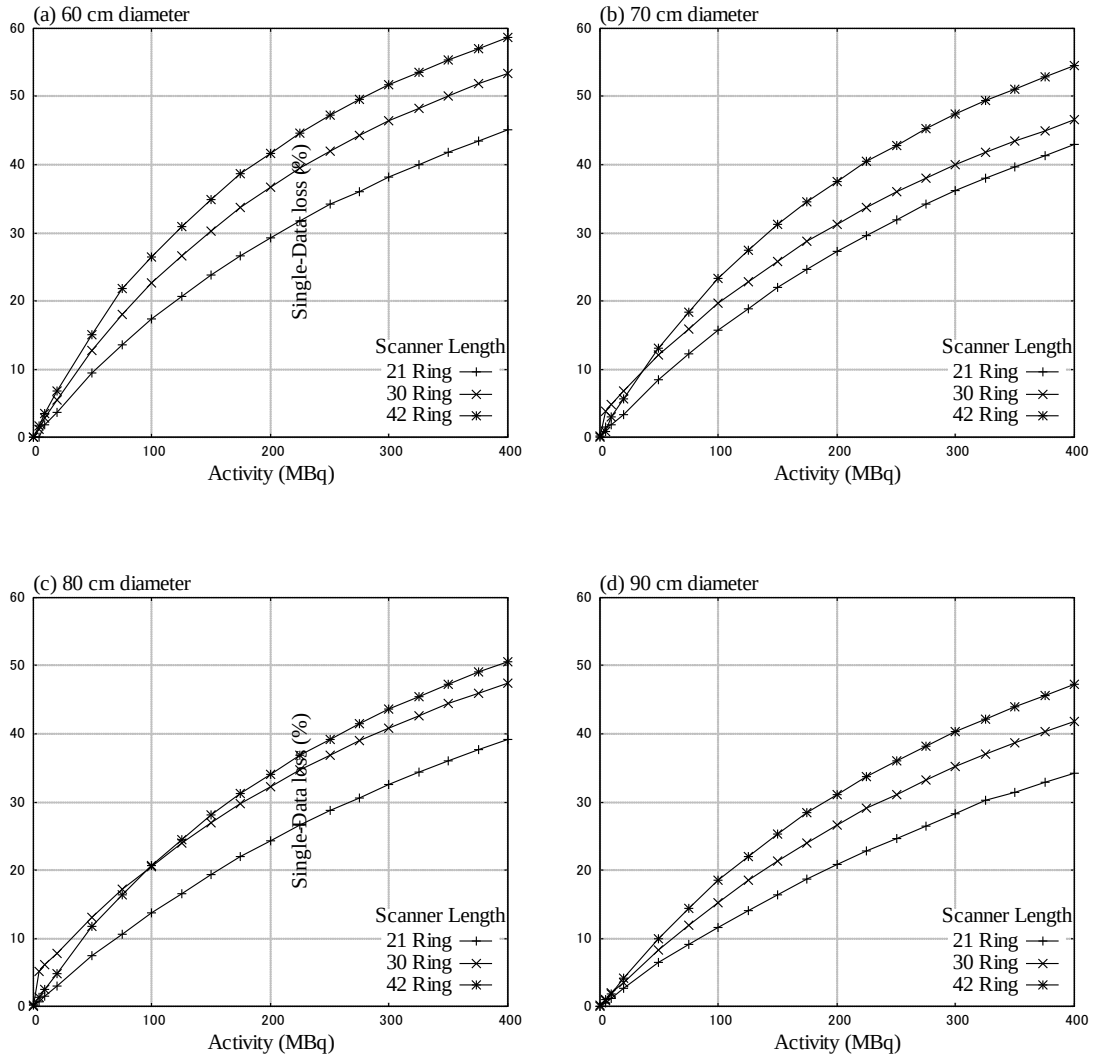

Figure 30 Single-data loss percentage suffered for every scanner. Graphs were grouped by its ring diameter.

In short, every scanner suffers a significant amount of single-data loss, especially smaller scanner PET. Figure 30 shown that scanner with 60 cm ring diameter, has the highest single-data loss in comparison to other scanners, which near to 60% for entire-body PET. This loss would off course, affect the number of true count for each scanner, and hence the NECR values.

5.3.3. Count Rate Performance

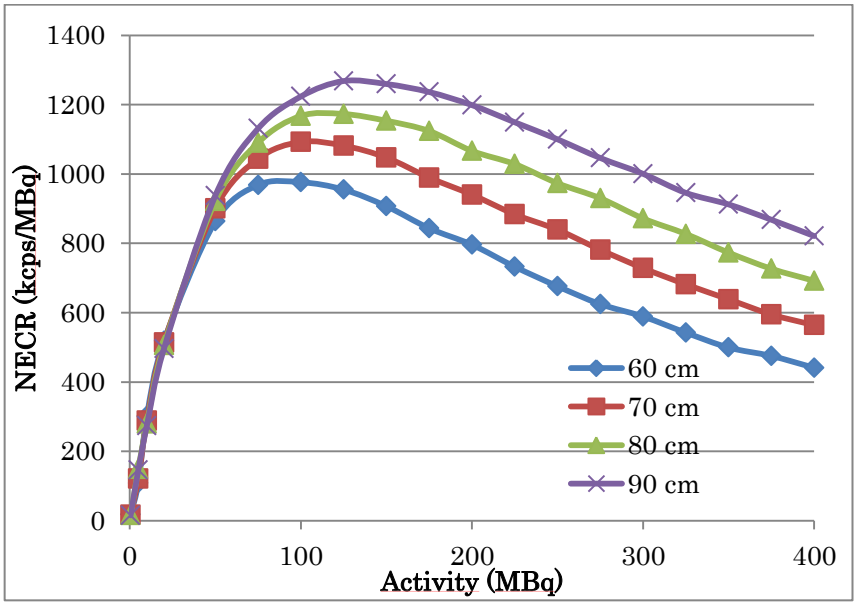

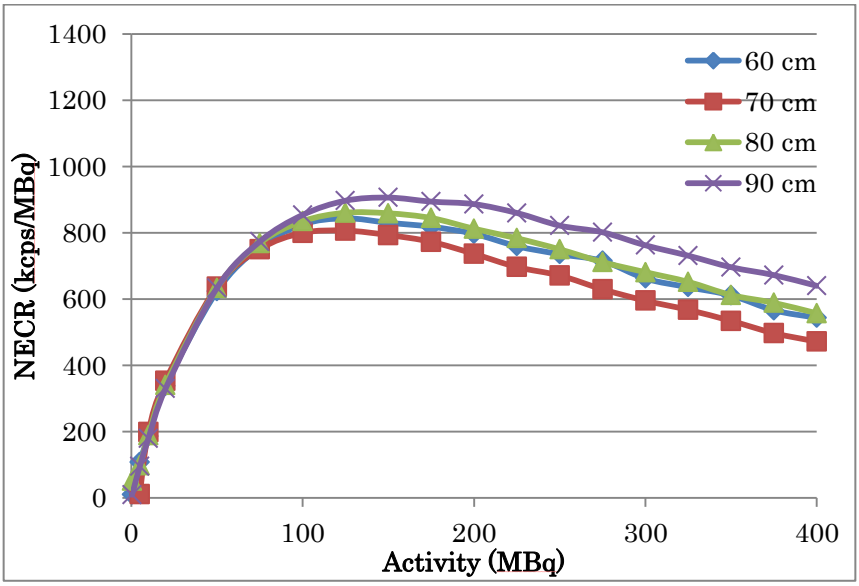

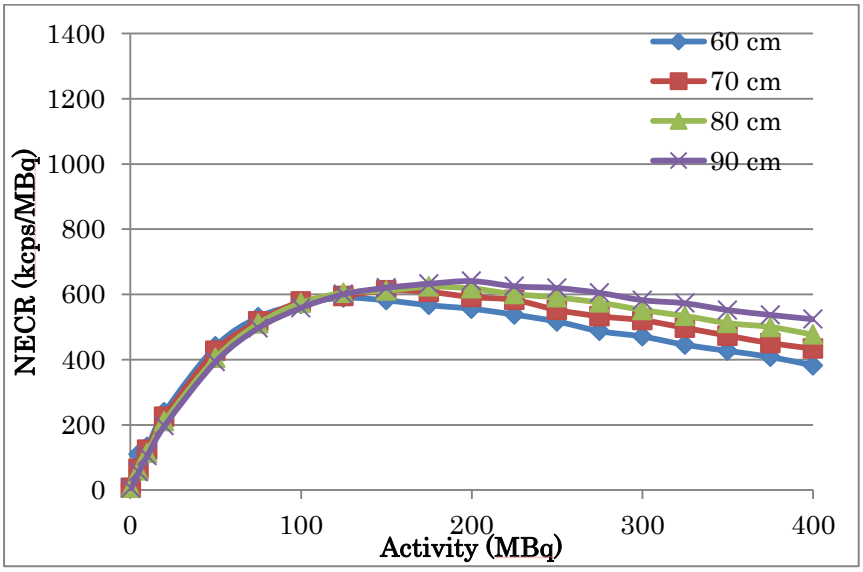

Figure 31 NECR values for different ring scanner when dead-time is applied for 42, 30 and 21 ring respectively (top to bottom). 60 cm ring diameter scanner which is supposed the highest peak among others, is found to be the lowest for entire-body PET.

Figure 31 on NECR graphs, describes that the NECR peak value is increasing, as the scanner length is extended from 100 cm up to 200 cm FOV length. However, while the smaller diameter scanner (60 cm) has a higher peak for 100 and 144 cm length scanner, it is not the case for 200 cm scanner. While we expect that smaller diameter would always have a higher NECR peak for any scanner length as it has higher sensitivity, larger scanner (90 cm) has the highest NECR peak values for 2-m long FOV. This is the effect of single-data loss suffered for each scanner due to the dead-time applied for individual detector as well as axially grouping dead-time. In summary Figure 32 describes the changes in the NECR peak values for different scanner length, in different ring diameters.

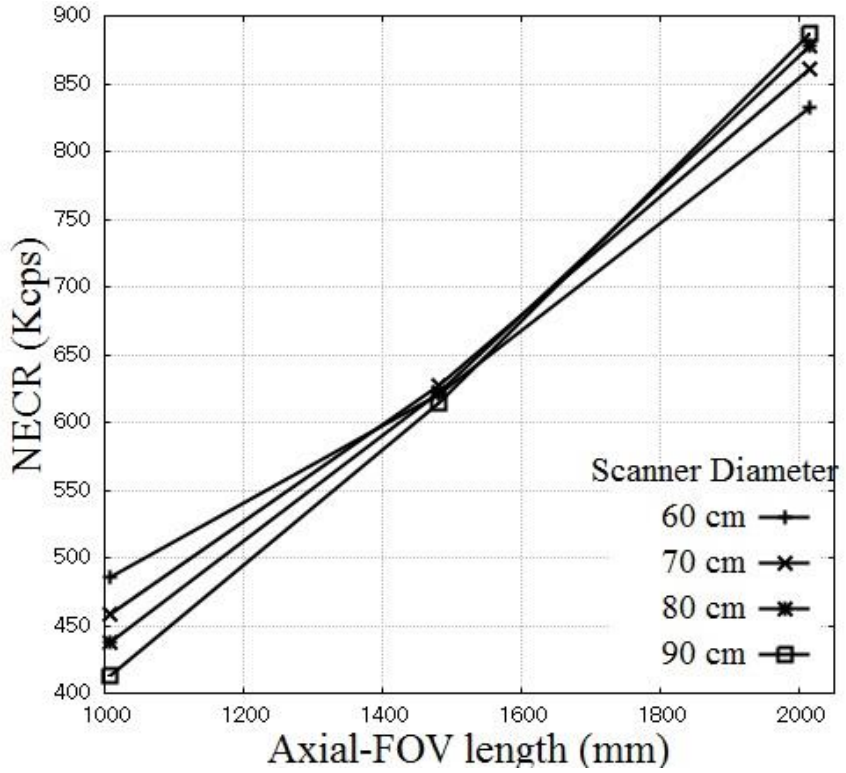

Figure 32 NECR peak values for different Axial-FOV length and different scanner diameter

5.3.3.1. NECR Without Grouping Dead-time

To show how much single-data is lost due to dead-time, one needs to remove the grouping dead-time. With the current design of detectors, we cannot avoid the individual dead-time belong to the each detectors. However, the dead-time for grouping axially stacked detectors could be arranged in a different manner. The single count as shown in Figure 33 is achieved without any group dead-time applied. In comparison to Figure 29, now the smallest diameter has the highest rate of single count as expected. This applied for all scanners with different axial FOV length.

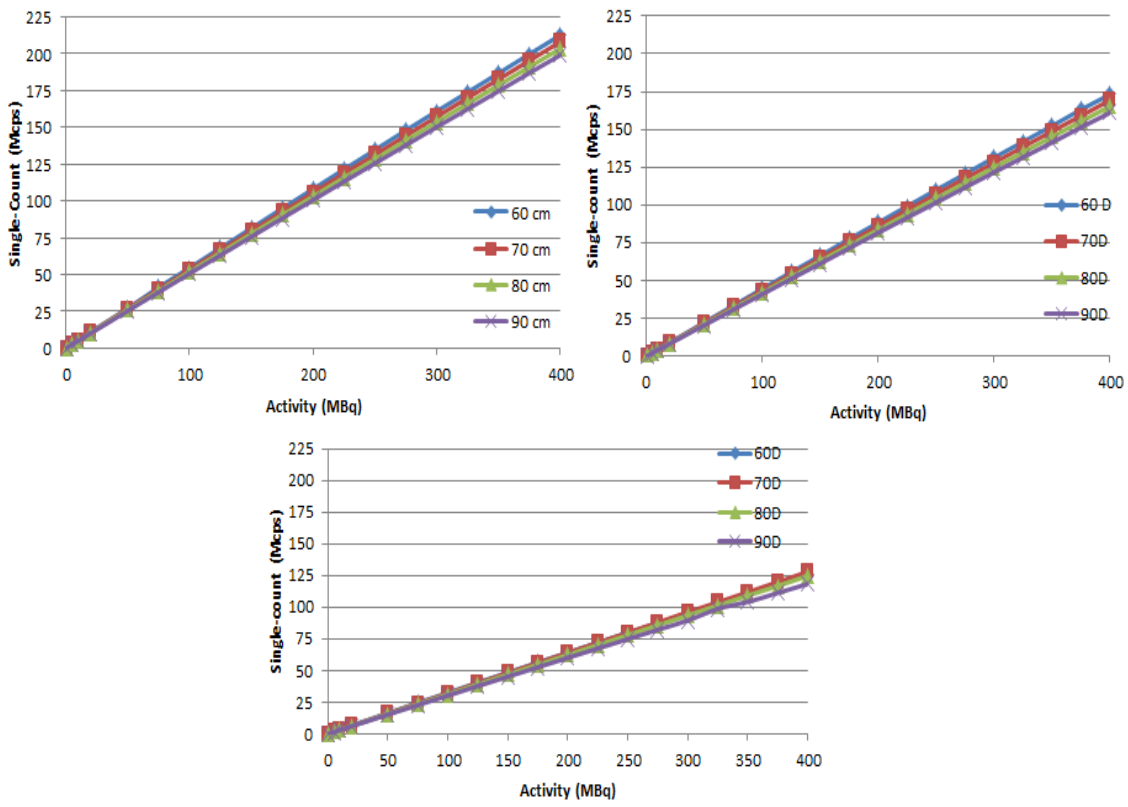

Figure 33 Single count of 3 different Axial-FOV PET (42, 30 and 21 ring from left to right) scanner without the grouping dead-time applied. Integration dead-time is unavoidable at this stage of scanner design

As we removed the dead-time grouping, we re-calculated the NECR values without dead-time loss for every scanner, as shown in

Figure 34. The value NECR peak is much higher than it was before. However, due to high random count, the value of NECR for 60 cm ring diameter scanner is lower.

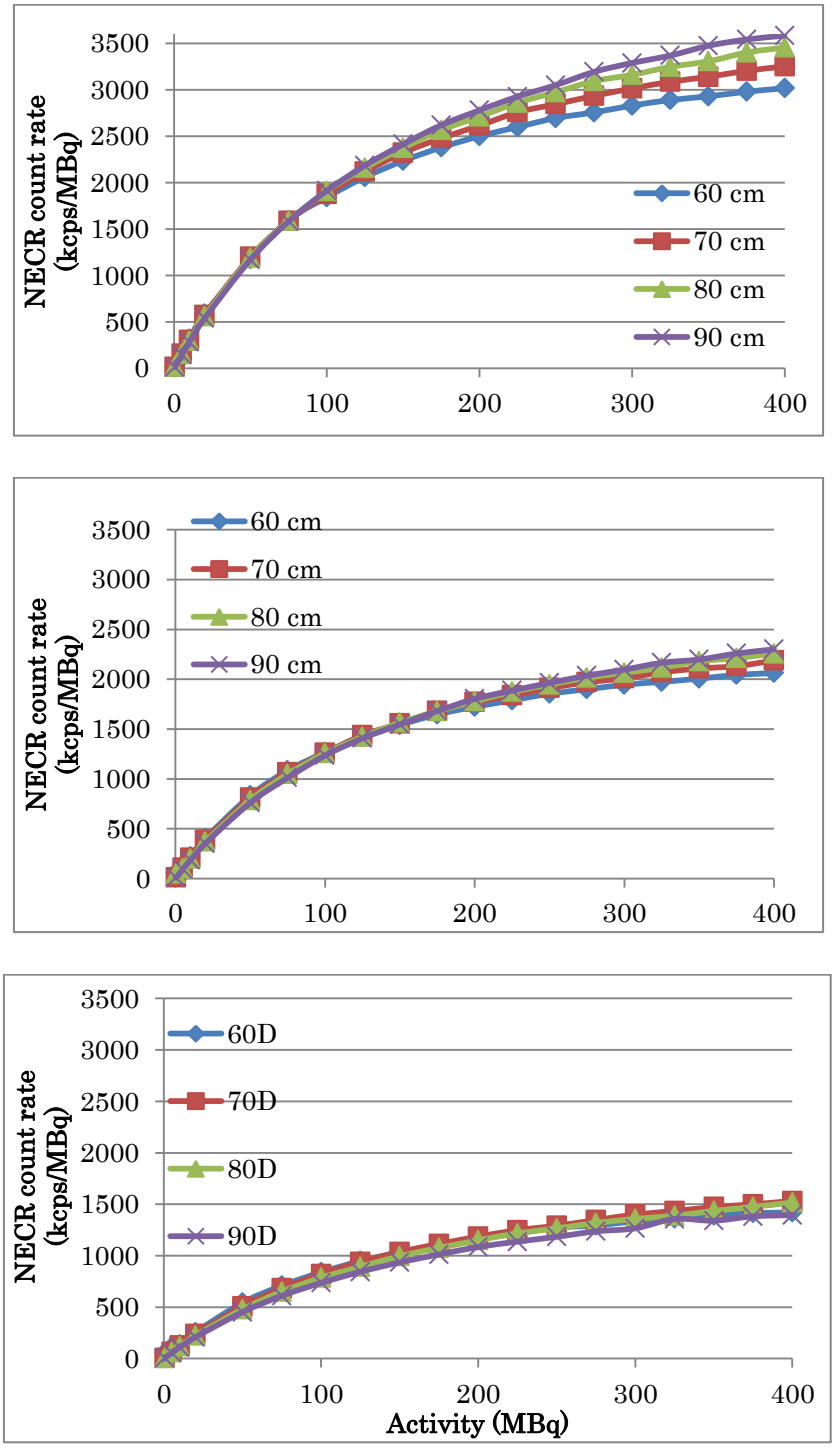

Figure 34 NECR values with no grouping dead-time for different scanner diameter for 42 (top), 30 (middle) and 21 ring (bottom) scanner.

5.3.3.2. NECR With 50% Dead-time

To minimize the effect of dead-time, we now use half value of the dead-time than it was before. When the grouping dead-time is given a value of 128 ns, the single-data loss rate for entire-body PET is improved as shown in Figure 35. Previously, the single-data loss of 256 ns grouping dead-time reached almost 60% for 60 cm ring diameter scanner, whereas now is reduced to 42%.

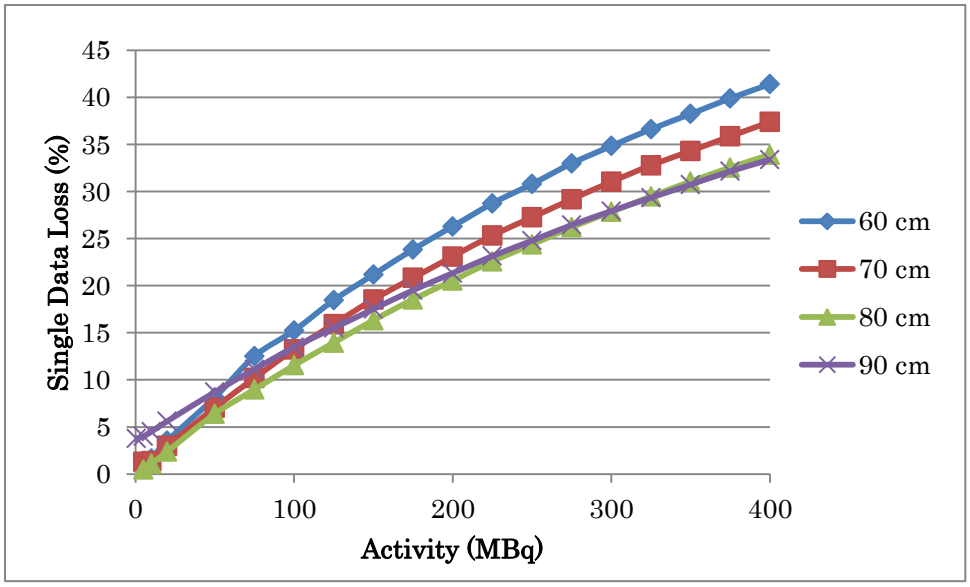

Figure 35 Single Data loss in percentage for entire-body PET with dead time of 128 ns (50%)

5.3.3.3. NECR With 3 Groups Axial Detectors

Some other arrangement can be made with the grouping non-paralysable dead-time. As Yoshida et.al. [26] described his method in arranging it in 3 different types namely *independent readout*, in which every coincidence circuit is connected to the every detectors; *whole-grouping* in which all axially stacked detectors is connected to as one group and the dead-time is applied; and

partial-grouping, for example by making a group of six axial detectors each. The result shows that the last grouping can mitigate single data collision into the grouping circuit. Scanner performance with the last grouping arrangement, even though lower than the ideal independent readout, can supersede the whole-grouping of axial-detectors. Hence the above result can further be improved with such grouping arrangement.

In this scanner design, we tried to group the axial-detectors into several groups as shown in Figure 36 and assigned the non-paralyzable dead-time to each of the group. Few different detectors grouping arrangements were made in which several axially detector was grouped into a separate coincidence sorter circuitry. Since the entire-body PET scanner has a total of 42 rings, we can only apply 2, 3, 6 and 7 grouping which correspond to 21, 14, 7 and 6 axially-arranged detectors in each group, respectively.

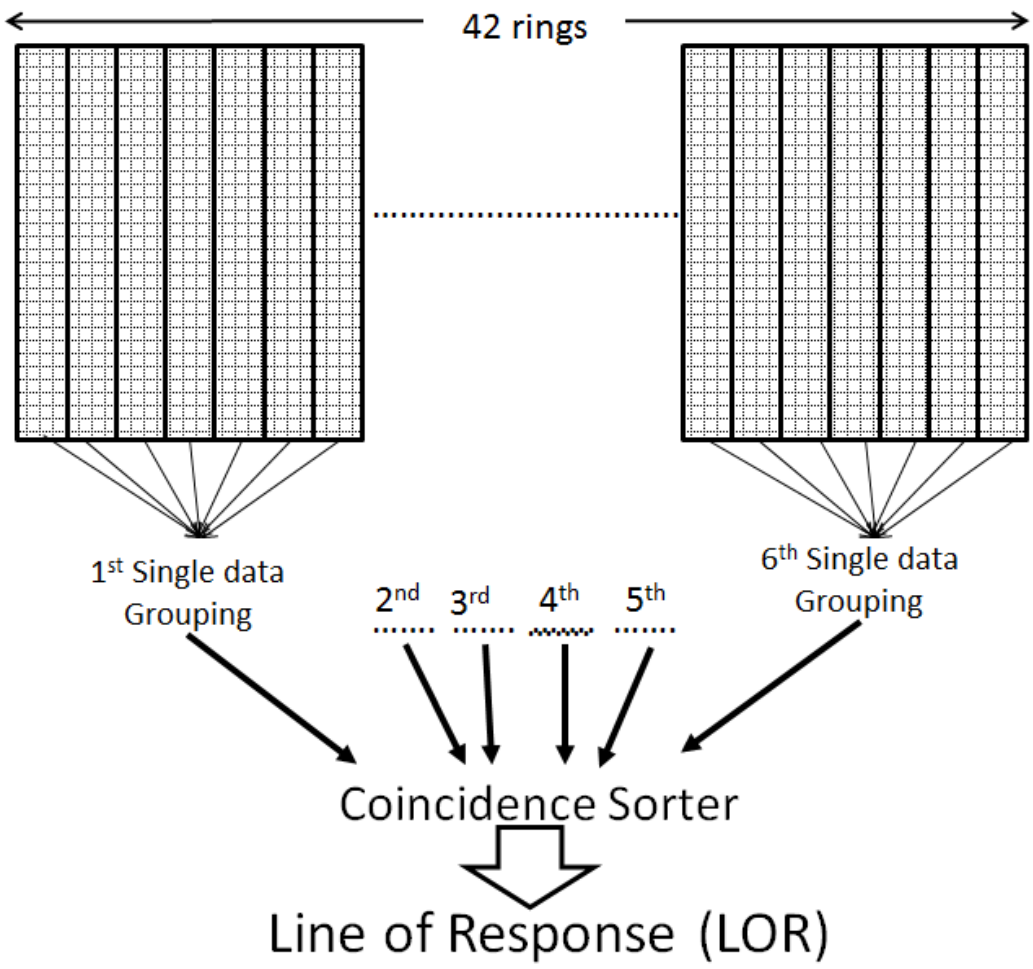

Figure 36 Grouping of several detectors to achieve a better data acquisition and reduce single-data loss

The NECR curves with different detector groupings are shown in Figure 37. As the number of grouping is increased, the NECRs were improved. However, larger detector grouping requires more complex coincidence sorter circuitry. Therefore, even though 7 grouping has the best performance in terms of NECR, we used 3 grouping setting in our simulations, since it would compromise both NECR values

as well as coincidence sorter circuitry required in the actual implementation.

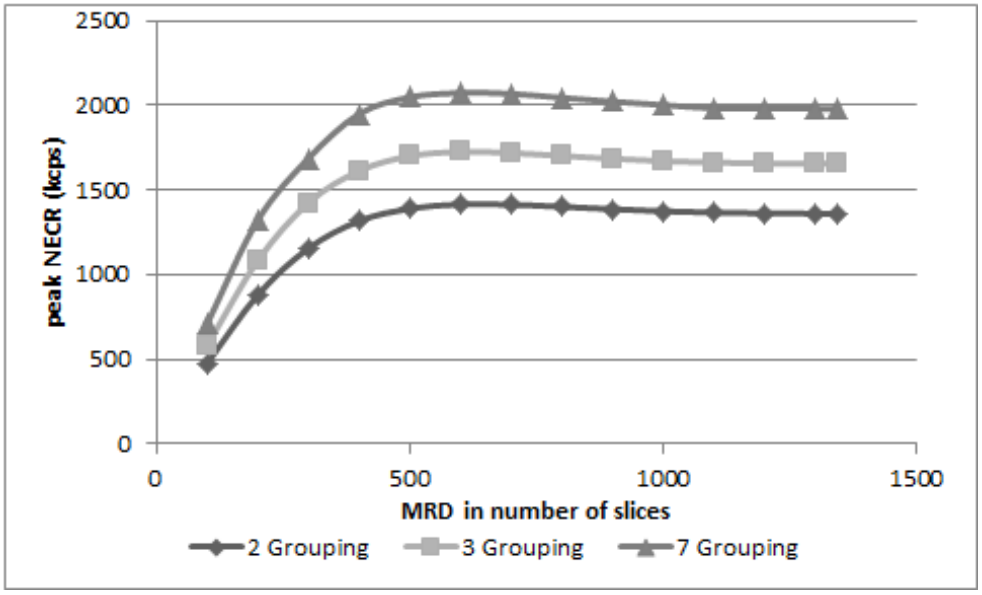

Figure 37 NECR curves for different detector grouping.

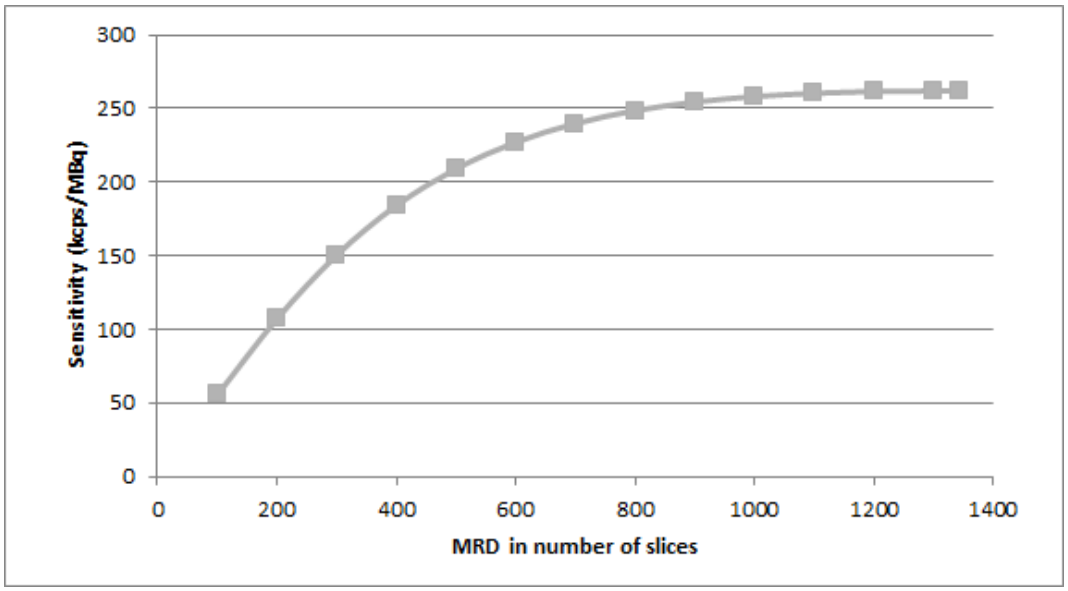

Figure 38 Total Sensitivity for different MRD

Figure 38 shows total sensitivity of the entire-body PET scanner as a function of MRD. The total sensitivity with the full MRD was 262 kcps/MBq. On the other hand, the total sensitivity with 600 MRD was 227 kcps/MBq. The total sensitivity with full MRD increased 15% than that with 600 MRD.

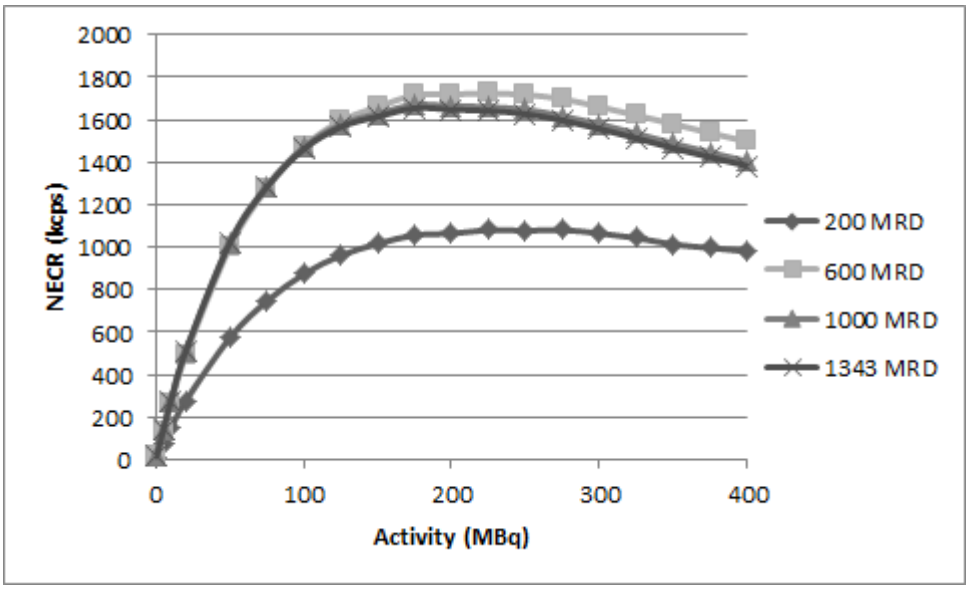

Figure 39 NECR curves for entire-body PET with 20 cm Phantom at several MRDs

Figure 39 shows the NECR curves of the entire-body PET scanner with the 20-cm diameter phantom. The peak NECR has it maximum value at about half of MRD, which is an increase of 4.2% in comparison to the full MRD. Figure 40 shows peak NECR as a function of MRD for 3 phantom diameters. It shows that for all sizes of phantom diameter, around 500-600 MRD the scanner has a slightly higher NECR in comparison to the full MRD's NECR. However, from that point the NECR values starts falling down

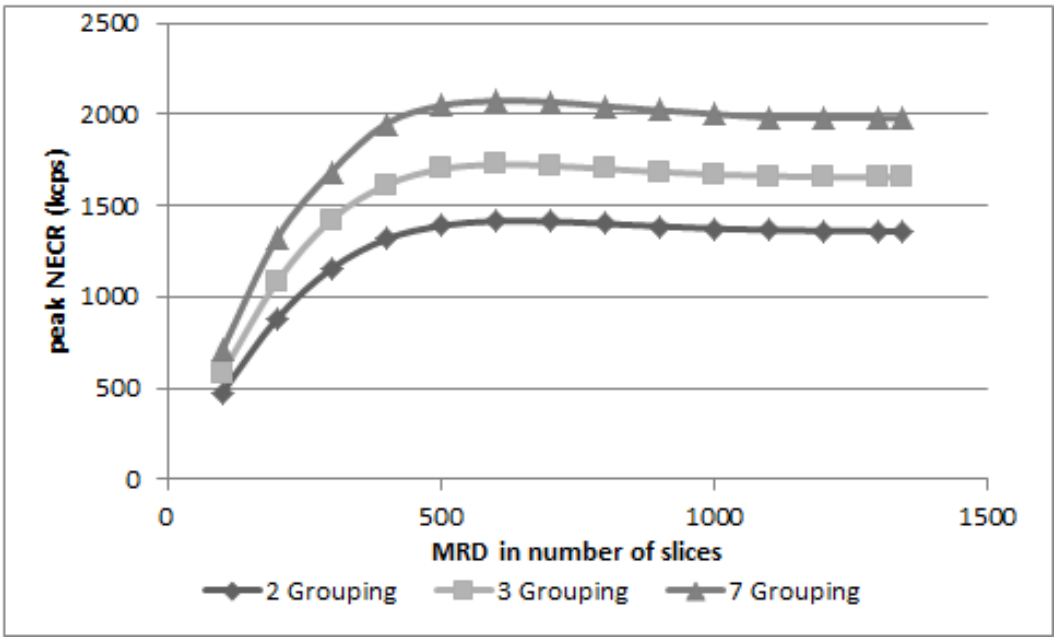

Figure 40 Peak NECR for different MRD for 3 types of phantom diameter.

5.4. Crystal Thickness

Some study has shown the choice of crystal thickness might change the performance of PET scanner [20], however there will be a trade-off with spatial resolution. Also, this value might not be similar for different scanner geometry. By reducing the crystal thickness, we could also reduce the development cost. Nevertheless, we have to be careful and observe the effect of minimizing crystal usage to the sensitivity and NECR values performance, especially for smaller ring diameter scanner. We used 2 other crystal thicknesses namely 16 and 12 mm which is arranged in 4-layer DOI. Figure 41 shows the relation between crystal thickness and its NECR values.

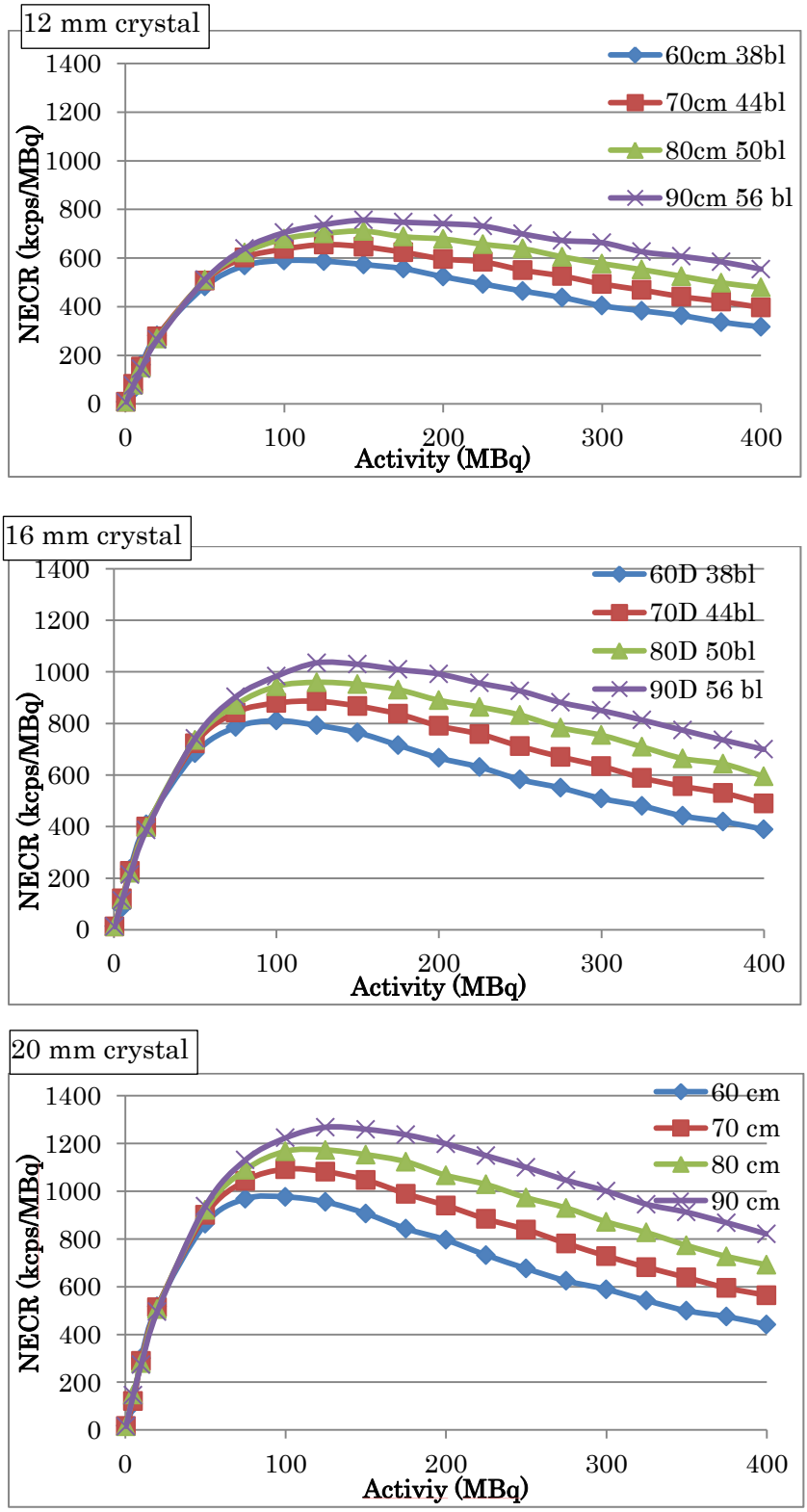

Figure 41 The affect of Crystal Thickness to NECR values

For all cases, the value of NECR is dropped up to 30-40% when a 12 mm crystal thickness is employed in the scanner, whereas a drop of NECR values up to 20-30% when 16 mm crystal thickness is utilized. Having smaller diameter scanner, in the case of thinner crystal, does not enhance the performance of the scanner. Table 12 also shows that the reduction in crystal thickness also reduced the sensitivities for all type of scanners geometries. Since smaller diameter in general has higher sensitivities, therefore 60 cm diameter scanner with 16 mm crystal thickness, the loss of sensitivities is only around 11%.

Table 12 Sensitivity (kcps/MBq) for different crystal thickness and its lost/gain (bracket)

Crystal Thickness	Ring diameter			
	90 cm	80 cm	70 cm	60 cm
20 mm	257.96	272.76	289.05	306.73
	(0.95)	(1.00)	(1.06)	(1.12)
16 mm	202.18	214.93	228.36	243.01
	(0.74)	(0.79)	(0.84)	(0.89)
12 mm	101.64	147.89	157.61	169.01
	(0.37)	(0.54)	(0.58)	(0.62)

5.5. Crystal Gap

Another method of reducing crystal volume in a scanner is by introducing a gap between detector rings as shown in Figure 42. In this simulation, the gap is varied from 1 up to 3 crystal gaps. As can be seen in Table 13, a gap of 3 crystals for entire-body PET could reduce a crystal volume up to 16.7% or a reduction of 7 detector ring.

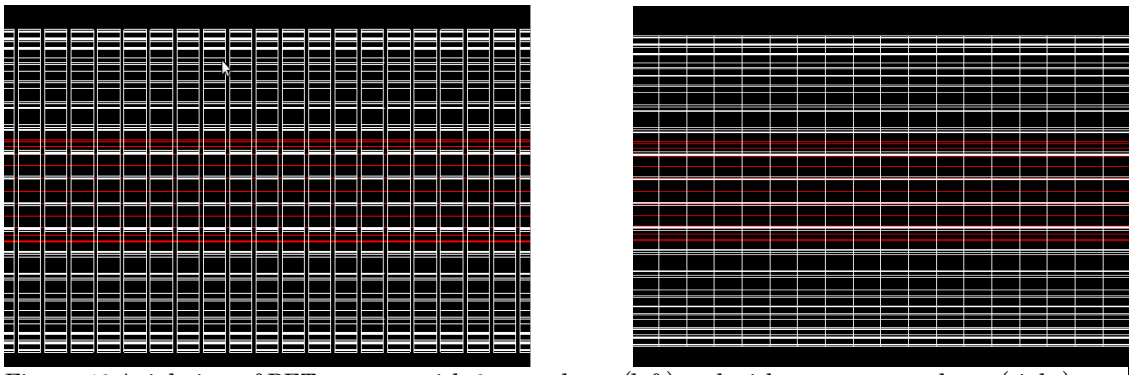

Figure 42 Axial view of PET scanner with 3 crystal gap (left) and without any crystal gap (right)

Table 13 Crystal volume reduction by introducing crystal gap between ring detector

No of crystal Gap	No of detector ring	Crystal reduction	Crystal Volume (litre)
1	39	7.15 %	63.8
2	37	11.9 %	60.54
3	35	16.7%	57.2

The sensitivity and count rate performance would surely affected by the reduction of crystal volume. Figure 43 shows an example how the sensitivity of 60 cm and 80 cm ring diameter scanner is getting lower as the crystal gap is increased.

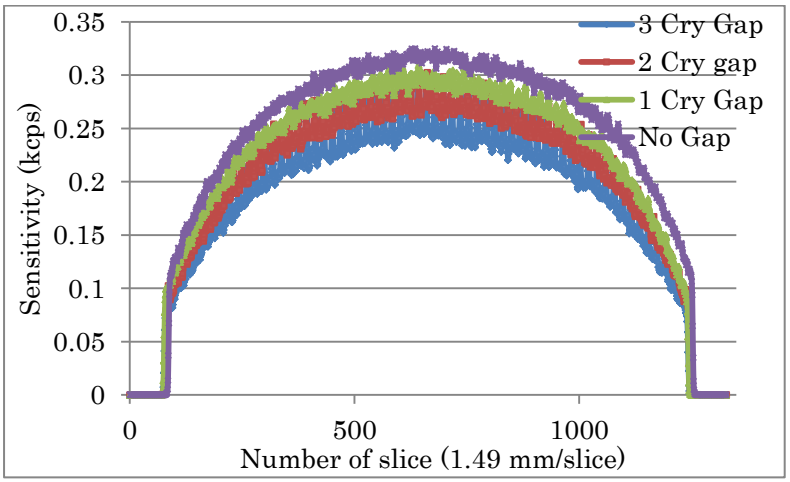

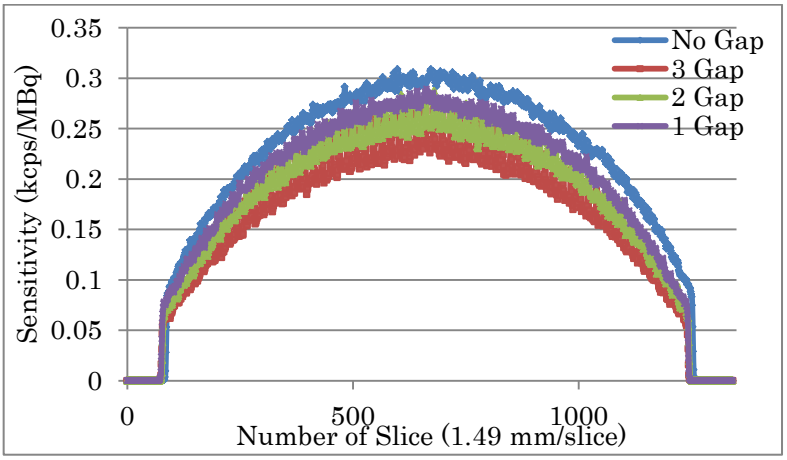

Figure 43 Sensitivity of 60 cm and 80 cm ring diameter scanner with the introduction of crystal gap between the ring detectors

While Figure 44 shows how the NECR peak values has been reduced around 10% every time 1 crystal gap is inserted between the detector rings. This happened for both 60 cm and 80 cm ring diameter scanner.

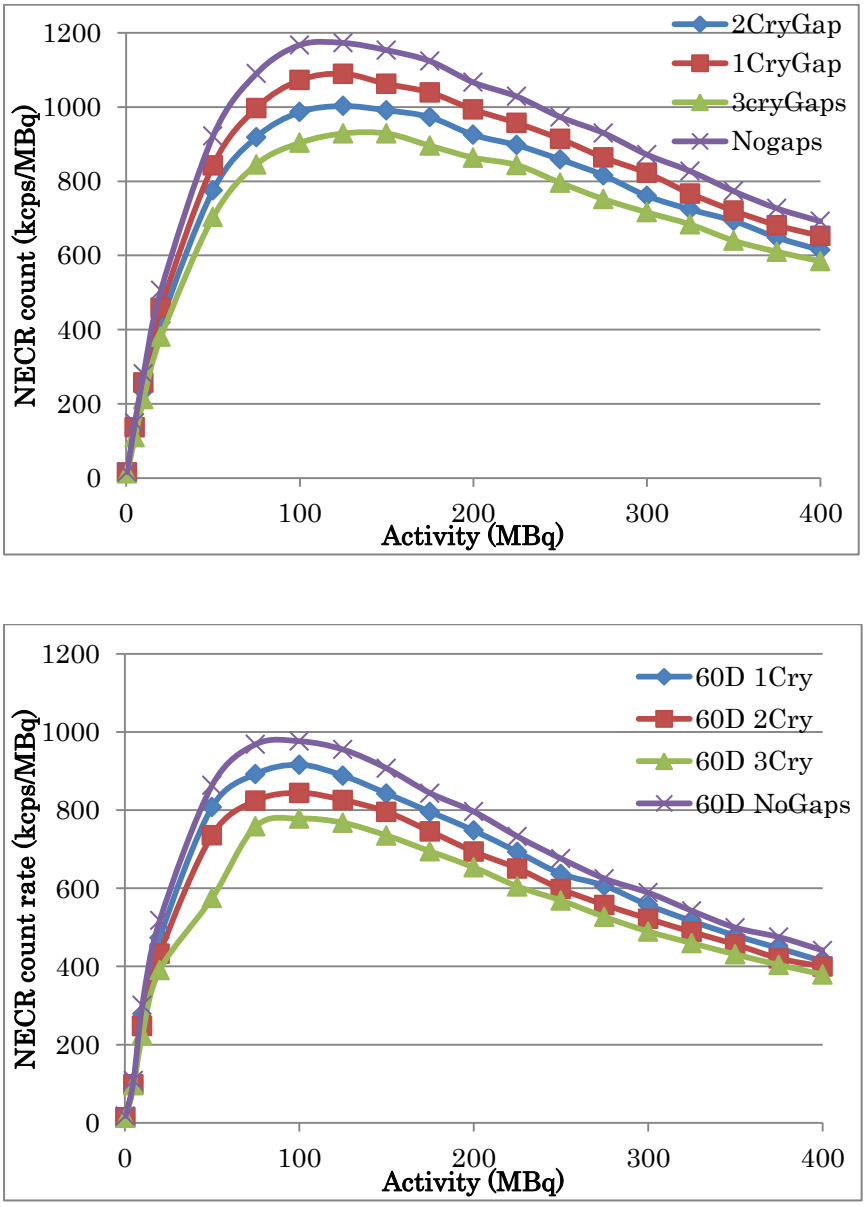

Figure 44 NECR values for 80 cm (top) and 60 cm ring diameter (bottom) PET scanner with different crystal gap between ring detectors.

5.6. Summary

The choice of smaller diameter for entire-body PET is desirable since it is promising a higher value of sensitivity as well as superior peak of NECR. However, smaller diameter seems to suffer from single-data loss due to dead-time grouping of axially stacked detectors, more than larger diameter scanner. Therefore, an arrangement should be made for minimizing this dead-time loss, by either reducing the amount of grouping dead-time or making a smaller group of axially stacked detectors with separate dead-time applied for each group.

Effort was also made to reduce the production cost for such entire-body PET, by reducing the volume of crystal used in the scanner. However, if we choose a thinner crystal or introducing gaps between the ring detectors, it sacrifices the both performances on sensitivity and count rate.

Chapter 6

Pros and Cons on Entire-body PET for Physical Examination

The 2-m long PET scanner with the conventional DAQ architecture promises a significant increase in both NECR and sensitivity compare to the conventional PET scanner. Also, the 2-m long PET scanner with 60-cm ring diameter could not only reduce number of detectors by 21% but also had 15% higher sensitivity compared to one with 80-cm ring diameter. On the other hand, despite higher sensitivity, the NECR of the 60-cm ring diameter was lower than that of the 80-cm ring diameter. This result from the single data loss for grouping axially stacked

detectors using the conventional DAQ architecture. In the 2-m long PET scanner with the conventional DAQ architecture, single data throughput was saturated in limited activity. As a result, single data loss at the grouping circuits were limited to the peak NECR for the entire whole-body PET scanner. To resolve this problem need to separate grouping processes in axial direction. But, coincidence detection circuits become complex.

Sensitivity profile of the conventional PET scanner had triangle distribution. As not only axial FOV extended and but also the ring diameter was narrow, sensitivity profiles came to a dome shape distribution. Conventionally, sensitivity of a PET scanner depends on detection efficiency and acceptance angle. This was because increase of an acceptance angle is saturated as the axial FOV is extended partially. Therefore, at the FOV center, saturation of the acceptance angle becomes to maximum effect. Also, oblique LORs sacrifice maximum sensitivity by maximum ring difference (MRD) in order to obtain a uniform sensitivity profile for the entire whole-body PET scanner. On the other hand, oblique LORs cause to the parallax error. The DOI detector can reduce the parallax error, but the entire whole-body PET scanner has extreme oblique LORs. Extremely oblique LORs may not contribute to imaging performance.

6.1. Data Size

The entire-body PET scanner would have to process a large amount of data

compared to conventional PET scanners. At activity of peak NECR, single count rate was 53.02 Mcps and this value is 6.3 times than the conventional PET scanner. Also, prompt and random count rate was 7.69 Mcps and this value is 26.94 times than the conventional PET scanner. Therefore, coincidence detection circuits need more parallel and high throughput performance. Also, total number of LORs with the 2-m long PET scanner with 80-cm ring diameter was over 130.4 Giga. This was 110.25 times than the conventional PET scanner. On the other hand, in the 2-m long PET scanner with 60-cm ring diameter, this value can be reduced by 0.62 times.The following Table 14 shows the number of LORs for different scanner length and different diameter.

Table 14 Number of LORs for different ring geometry

Data size Increase (based on conventional scanner)				
	90 cm	80 cm	70 cm	60 cm
42 ring	138.60	110.25	85.14	63.27
30 ring	70.71	56.25	43.44	32.28
21 ring	34.65	27.5625	21.23	15.82
4 ring	1.26	1	0.77	0.57

Hence, reducing the diameter into 60 cm, has actually reduced the amount of data by almost 40% while keeping the sensitivity as well as high peak of NECR values

6.2. Parallax Error

By extending the axial-FOV of a PET device, it means introducing a great amount of Line of response (LORs), especially oblique LOR. This in fact become one of the detrimental point of Entire-body PET design, since the data size to be

processed for image reconstructions will be very big as well as it will introduced parallax error. Nevertheless, due to the implementation of DOI detectors which keep high spatial resolution, this problems could be resolved.

6.3. Time Savings

With a simple calculation, we can predict the scanning time for individual scanner to achieve similar sensitivities

Table 15 Time savings per scanner in comparison to conventional PET

	Ring diameter			
	90 cm	80 cm	70 cm	60 cm
42 ring	0:00:29	0:00:27	0:00:26	0:00:24
30 ring	0:00:47	0:00:44	0:00:41	0:00:38
21 ring	0:01:26	0:01:19	0:01:12	0:01:05
4 ring	0:34:19	0:30:00	0:26:29	0:22:59

With time saving of 20-30 min scanning per patient for a PET/CT for example, it has increased the number of patient up to 40%. [31]. Hence clinical centers can have more patients examined daily, which means faster return value of such equipment. When scan time of the conventional PET scanner is 30 min, scan time of the 2-m long PET scanner with 60-cm ring diameter can be reduced to 25 s by simple calculation. This PET scanner may be cost effective for clinical PET scanners with high scan throughput.

Using the 60 cm diameter PET scanner as a base, taking into considerations the bed movement to shift the patient in and out the scanner, other preparation time,

we can say that every patient might need of 5 min total treatment time (time between the injected dose until treatment is not considered here). Hence, based on the assumption that the device can be used continuously for 8 hours a day, and an arrangement of parallel patient (one patient to get injection 10 minutes after the previous patient), we can have a dramatically increasing number of patient, up to 96 patients per day, while today's today clinic mostly can only take up 10-16 patients daily. Hence, this sub-minute acquisition time is a great motivating factor for Entire-body PET development.

6.4. Cost Savings

Cost is the most important problem. Table 16 below shown the number of crystal used for every scanner's geometry we used in this experiment. The number of crystal volume used, is increasing as the number of ring extended. However, by choosing a smaller diameter 60 cm for example, there will be a saving up to 24% of crystal used compared to standard diameter 80 cm.

Table 16 Number of crystal used in every geometry

No of ring	Ring diameter			
	90 cm	80 cm	70 cm	60 cm
42 ring	602112	537600	473088	408576
30 ring	430080	384000	337920	291840
21 ring	301056	268800	236544	204288
4 ring	57344	51200	45056	38912

Another alternative to overcome this cost issue is the OpenPET scanner [32-34]. Its design is introducing gaps between the ring in order to reduce the number of

crystal involved, but at the same time compromising the sensitivity value, NECR, cost and dose injected to the patient. The number of crystal used for the same length of scanner varies according to the design,

6.5. Physical Examination With the benefit of short scanning time and high sensitivity, we can apply a low injected dose for patient. Currently, the FDG-PET screening test is utilizing 261 MBq (for men) or 205 MBq (for women) radionuclide for a dedicated PET. As the half-time of FDG^{18} is approximately 2 hours, and the waiting time between injection and scanning is 30-60 minutes, by the time the test is conducted, the value of activity is half of the given dose. Based on the research of Japan FDG-PET cancer screening test, most of the equipment utilized having an axial FOV of less than 20 cm, which NECR peak around 300-400 MBq. Whereas the entire-body PET reach the peak of count rate at around 125 MBq, which is almost half of the current given dose. Therefore, the entire-body PET could detect cancer in higher probability.

Moreover, due to short scan time interval, even by giving lower dose to patient, the activity of radionuclide at the time of scanning will still fall within the peak area of NECR. Hence, by giving a dose of 125MBq, for example, or equal to 1.8MBq/kg, the cancer would likely be detected.

6.6. Other Factors

Still there are other factors which also influence the sensitivity as well as NECR values such as stopping factor of the detector and scintillator absorption value and other recent development of detectors [19-21]. To limit the scope of the research, we have not involved these factors yet. However, we believe that, with all these factors taken into account while developing entire-body PET, the sensitivity and NECR values can be further improved.

Chapter 7

Conclusion

The design of entire-body PET with smaller diameter (60 cm) has achieved a 17% higher sensitivity compared to one with 80-cm ring diameter and it has reached an NECR peak of 835 kcps at 125MBq. This also means a gain of sensitivity and NECR about 80 and 15 times respectively, in comparison to the conventional 4 rings 80 cm ring diameter scanner.

This fact brings further benefit of time saving of individual scanning per patient, which can be drastically reduced down to 20-30 sec per patient, for the same level

of sensitivity achieved by the conventional PET scanner.

This type of scanner would be suitable for a physical examination such as FDG-PET cancer screening test, since it offers few interesting feature:

- The short scanning time, which can increase the number of patients served daily from 16 patients a day (30 min per scan, 8 hours a day) up to 96 patients daily with 5 minutes scanning time.
- Lower injected dose can be given to patients of 1.8 MBq/kg for 70 kg patients or around 125 MBq where the scanner reaches the NECR peak value. This equal to 2.375 mSv effective dose. In contrast, the conventional PET scanner reached its NECR peak values at around 300-400 MBq, with effective dose of 4.4 mSv for PET, 10mSv for CT scan and 13.5 mSv for PET/CT.
- Due to its shorter scanning time and lower injected dose, automatically it is safer for healthy patient to take part in the screening test, even if the test need to be repeated after a certain time.
- Since the scanner cover the whole body at the same time, it can dynamically scan various organ with the same level of radionuclide activity. Hence, the possibility of detecting cancer at the first screening test will be higher and therefore less repeated test is required.

Even though the development cost might still be the main concern. However, the idea of smaller scanner would minimize the cost of the development by at least 21%. Moreover, if we combine the idea of introducing gaps between

ring detector and choosing a thinner crystal detector, the crystal volume involved will be further reduced.

Problem with small diameter entire-body PET scanner of single-data loss due to dead-time architecture in the conventional DAQ system, can be minimized by removing grouping dead-time (ideally), or minimizing the dead-time value. We can also have a separate arrangement for grouping detectors stacked in axial direction, which is proven to decrease the percentage of single-data loss suffered.

Another alternative to overcome these issues is the OpenPET scanner [32-34]. Its design is introducing gaps between the ring in order to reduce the number of crystal involved, but at the same time compromising the sensitivity value, NECR, cost and dose injected to the patient. The number of crystals used for the same length of scanner varies according to the design.

Bibliography

1. Karakatsanis N. A., et. al. Dynamic Multi-Bed FDG PET Imaging: Feasibility and Optimization. In Proceeding IEEE NSS-MIC 2011;3863-3870
2. Couceiro M, Ferreirac N C, Fonte P. Sensitivity assessment of wide Axial Field of View PET systems via Monte Carlo simulations of NEMA-like measurements. Nucl Instrum Methods Phys.,2007;A580:485-488.
3. Eriksson L, et.al.. An investigation of sensitivity limits in PET scanners. Nucl Instrum Methods Phys. 2007; A 580:836-842.
4. Eriksson L, et.al. Towards Sub-Minute PET Examination. IEEE Trans. Nucl Sci Feb 2011;58(1):76-81.
5. Crespo P. et al. Whole-body single-bed time-of-flight RPC-PET: simulation of axial and planar sensitivities with NEMA and anthropomorphic phantoms. Nucl. Instrum. Conf. Rec; 2009.p.3420-3425.
6. Adam L-E, Karp J S., Daube-Witherspoon M E. and Smith R J., Performance of a Whole-Body PET Scanner Using Curve-Plate NaI(Tl) Detectors. The Journal Nucl Med; Dec 2011 ; 42(12):1821- 1830

7. Saha G B. Performance Characteristic of PET scanner In: Basic of PET Imaging: Physics, Chemistry and Regulations. Springer, 2010.;97-116.
8. Murayama H., Ishibashi H., Uchida H., Omura T., and Yamashita T., Depth encoding multicrystal detectors for PET. IEEE Trans. Nucl. Sci.,1998;45(3):. 1152–1157..
9. Lee JW, Kang KW, Paeng JC, Lee SM, Jang SJ, Chung JK, et al. Cancer screening using 18F-FDG PET/CT in Korean asymptomatic volunteers: a preliminary report. Ann Nucl Med. 2009; 23:685–91
10. Tsuda .T. *et al.*, Performance evaluation of a subset of a four-layer LSO detector for a small animal DOI PET scanner: jPET-RD. IEEE Trans. Nucl. Sci. 2006;53(1); 35–39.
11. Takeshi M. et.al, Radiation exposure and risk–benefit analysis in cancer screening using FDG-PET: results of a Japanese nationwide survey. Ann Nucl Med (2011) 25:657–666
12. Ryogo M., Performance profile of FDG-PET and PET/CT for cancer screening on the basis of a Japanese Nationwide Survey Ann Nucl Med (2007) 21:481–498
13. Ryogo M., Analysis of various malignant neoplasms detected by FDG-PET cancer screening program: based on a Japanese Nationwide Survey Ann Nucl Med (2011) 25:45–54
14. Seiei Y.,Michiru I., PET and cancer screening Annals of Nuclear Medicine Vol. 19, No. 3, 167–177, 2005

15. Knoll, G. Radiation Detection and Measurement; Wiley: New York, NY, USA, 2001

16. Valentine J., International Commission on Radiological Protection. Radiation dose to patients from radiopharmaceuticals, ICRP Publication 80, Addendum to ICRP 53,. Oxford: Pergamon Press;1998.

17. National Electrical Manufacturers Association, Performance Measurements of Positron Emission Tomographs, NEMA Standards Pub. NU 2--2007, , Rosslyn, VA, National Electrical Manufacturers Association ; 2007

18. Leo,W R. Techniques for Nuclear and Particle Physics Experiments: A How-To Approach, Springer, 1994, p 122-125

19. Hao P. and Craig S. L., Recent Developments in PET Instrumentation, Current Pharmaceutical Biotech, 2010; 11: 555-571

20. Surti S, Lee E, Werner M E, Karp J S. Imaging study of a clinical PET scanner design using an optimal crystal thickness and scanner axial FOV. In,

21. Karakatsanis N, Nikita K. A simulation model of the counting-rate response of clinical pet systems and it's application to optimize the injected dose. IEEE Int. Symp. Biomed. Img; 2009: 398-401.

22. Yoshida E., Yamaya T., Watanabe M., Inadama N., Ayako K., Tsuda T., Kitamura K., Hasegawa T., Obi T., Haneishi H. and Murayama H.. Design and initial evaluation of 4-layer DOI-PET System : the jPET-D4. Japanese Journal of Medical Physics, Feb 2006; 26(3); 131-40

23. Yamaya T., Hagiwara N., Obi T., et.al., ”Transaxial system models for the jPET-D4 image reconstruction,” *Phys. Med. Biol,*. vol. 50, pp. 5339-5355, 2005.

24. Yamaya T., Hagiwara N., Obi T., et al., “Preliminary performance evaluation of the prototype system for a brain DOI-PET scanner: jPET-D4”, Conf. Rec. 2003 IEEE NSS & MIC, M2-285, 2003

25. Yoshida E., Yamaya T., Watanabe M., et.al, The jPET-D4: Detector Calibration and Acquisition System of the 4-layer DOI-PET Scanner. 2005.; IEEE NSS/MIC Conf.Rec M11-270; 2628-31

26. Yoshida. E, Yamaya T, Fumihiko N., Naoko I., Hideo M. Basic study of entire whole-body PET scanners based on the OpenPET geometry. Nucl. Instrum. Methods Phys. Res. 2010; A 621:576-580.

27. Orita N, Murayama H, Kawai H, et al., Three-dimensional array of scintillation crystals with proper reflector arrangement for a depth of interaction detector, IEEE Trans Nucl Sci.;2005; 52(1):8-14

28. Buvat I and Lazaro D. Monte Carlo simulations in emission tomography and GATE: An overview. Nucl. Instrum. Methods Phys. Res. A. 2006 S; A569:323-329.

29. Jan et al. GATE: A simulation toolkit for PET and SPECT. Phys. Med. Biol. 2004;49:4543-4561.

30. Assie K et al. Monte Carlo simulation in PET and SPECT instrumentation using GATE. Nucl. Instrum. Methods Phys. Res. A, 2004;A527:180-189.

31. Muhammad W. S., Ifigenia T., Nektaria M., Kostas S., Role and Cost Effectiveness of PET/CT in Management of Patients with Cancer, Yale J Bio Med 83. 2010;, 53-65.

32. Yamaya T, Inaniwa T, Minohara S, Yoshida E, Inadama N, Nishikido F, Shibuya K, Lam CF, Murayama H. A proposal of an open PET geometry, Phys.Med.Bio. 2008; 53(3): 757-77

33. Yoshida E, Yamaya T, Shibuya K, Nishikido F, Inadama N, and Murayama H. Simulation study on sensitivity and count rate characteristics of "OpenPET" geometries. IEEE Trans Nucl Sci Feb 2010;57(1):111-116.

34. Yoshida E, Yamaya T, Fumihiko N., Inadama N.. and Murayama H.. Feasibility study of entire whole-body PET scanners based on the OpenPET geometry, In Proceeding IEEE NSS-M 2009: 3628-3629

Citations to Previously Published Work

Large portions of this thesis have appeared in the following papers:

Refereed Publication (Full Paper) in Journal

Ismet Isnaini, Takashi Obi, Eiji Yoshida, Taiga Yamaya, “Monte-Carlo simulation of 2m-long PET scanners: benefits to sensitivity and NECR”, Radiological Physics and Technology Journal, accepted 24 December 2013, DOI 10.1007/s12194-013-0253-y

Ismet Isnaini, Takashi Obi, Eiji Yoshida, Taiga Yamaya, “Simulation of Sensitivity and NECR of Entire-body PET Scanners for different FOV diameters”, Nuclear Instruments and Methods in Physics Research A 751 (2014) 36-40

Refereed Publication in International Conference

Ismet Isnaini, Takashi Obi, Eiji Yoshida, Taiga Yamaya, “Simulation of Sensitivity and NECR of Entire-body PET Scanners for different FOV diameters”, 2013 IEEE MIC Conference, Seoul 27th Oct – 2nd Nov 2013

Publication at domestic conference and symposium

Ismet Isnaini, Takashi Obi, Eiji Yoshida, Taiga Yamaya, “Monte-Carlo simulation of a novel 2 m-long entire-body PET scanner”, IEICE Technical Report Vol 112 No 411 p.105-108 , Jan 2013,

Ismet Isnaini, Takashi Obi, Eiji Yoshida, Taiga Yamaya, "Monte-Carlo simulation of sensitivity and NECR of a 2m-long PET scanner," 医学物理 Japanese Journal of Medical Physics (第 105 回日本医学物理学会学術大会報文集), p. 139, 2013/4/13. (パシフィコ横浜)